Masters Theses

Graduate School

5-2017

Z Deviation Based Demand Side Control to Reduce FIDVR

Derek Brittian Lusby
University of Tennessee, Knoxville, dlusby1@vols.utk.edu

To the Graduate Council:

I am submitting herewith a thesis written by Derek Brittian Lusby entitled "Z Deviation Based Demand Side Control to Reduce FIDVR." I have examined the final electronic copy of this thesis for form and content and recommend that it be accepted in partial fulfillment of the requirements for the degree of Master of Science, with a major in Electrical Engineering.

Kevin L. Tomsovic, Major Professor

We have read this thesis and recommend its acceptance:

Seddik M. Djouadi, Fangxing Li

Accepted for the Council:
Dixie L. Thompson

Vice Provost and Dean of the Graduate School

(Original signatures are on file with official student records.)

Z Deviation Based Demand Side Control to Reduce FIDVR

A Thesis Presented for the

Master of Science

Degree

The University of Tennessee, Knoxville

Derek Brittian Lusby

May 2017

This thesis is dedicated to my parents, David and Beth Lusby, for their incredible love and support throughout my 23 years of life. Thank you for putting up with so many nights of me working down in the basement, and for providing in such an indescribably generous way for me.

Acknowledgements

First and foremost, I would like to thank God for blessing me with this wonderful opportunity to grow not only academically, but in all walks of my life. None of this would be possible without Him, and this process has been the catalyst for immeasurable growth in my life.

I would like to thank my parents, David and Beth, for their continuous support, both with a place to live as well as the love and emotional support you have shown me my entire life. You have pushed me to be the best that I can be, and I wouldn't have made it to this point without you.

I thank Dr. Tomsovic for the his time, guidance, and contributions into my research, as well as the opportunity to do this research. I also thank him for his work as my advisor throughout all of my graduate studies. I would also like to thank Dr. Tomsovic's research group for being so kind and inviting to me.

I would like to thank my management at Y12, Dave Harvey and Eric Taylor, as well as Ashley Stowe for their encouragement in my studies and for being so patient and helpful throughout the process.

Last but not least, I would like to thank my family and friends who have been such a tremendous source of encouragement throughout this process. I cannot say how much your prayers and support have meant to me.

"Who is it that overcomes the world except the one who believes that Jesus is the Son of God?"

1 John 5:5

"I can do all things through him who strengthens me."

Phillipians 4:13

Abstract

Accurate load modeling is key to depicting realistic system behavior in power system simulations. In the past, the use of static load models resulted in overly optimistic results, which led to unforeseen outages and issues following faults. One common cause of these types of unforeseen issues is Fault Induced Delayed Voltage Recovery (FIDVR). FIDVR occurs due to the stalling of single-phase residential air conditioners (A/C), and causes the voltage recovery after a fault to be slow. Improvements in load models over time have resulted in the capability of modeling load dynamics, and therefore better FIDVR.

A composite load model based on real world composition data is applied to a 179 bus system representing the WECC system. Then through mathematical derivation and fault analysis, a method, Z Deviation, is proposed as a way to identify the occurrence of FIDVR. Z Deviation is then implemented in a control scheme used to improve voltage recovery following FIDVR, and its effectiveness is compared to a device level protection scheme.

Table of Contents

List of Tables

List of Figures

Chapter 1

Introduction

1.1   The Role of Accurate Modeling

The ultimate goal of the power system is to successfully deliver sufficient power to meet the total end demand. In order to accomplish this goal, the power system must remain stable. Contingencies, such as line or bus faults, generator loss, and other outages, can lead to instability; as such the system must be equipped to deal with these disturbances. Vital in being prepared for these types of issues is the ability to model the system via software. Through this, tests can be conducted to investigate various scenarios and see what measures need to be taken to ensure adequate performance of the system.

The components that comprise the power system are diverse and have unique behavior, so accurate modeling may be difficult. This is especially true for modeling the various loads present in the system. Traditionally, loads were modeled with a static load model used to represent a wide variety of loads that were present in the real system. While this technique would prove sufficient for some loads and in some cases, the static models could not capture the dynamic behavior of some loads, such as induction motors. This static modeling of dynamic loads caused inaccuracies in system models, which then led to unexpected issues. This dilemma was especially

prevalent in cases involving what is now know as Fault Induced Delayed Voltage Recovery.

1.2 Fault Induced Delayed Voltage Recovery

Fault Induced Delayed Voltage Recovery (FIDVR) is an issue that can threaten the voltage stability of the power system. Due to the behavior of residential air conditioners and their prevalence in certain areas at certain times, they can prevent voltages within the system from recovering quickly following a contingency. Before the advent of modern load models, the static load models of the time could not capture the unique behavior of these motors. Thus, there are multiple instances when simulations showed that the system would recover quickly after a fault, but failed to do so in the real system. Many of the events, some which will be discussed in the paper, have been able to retroactively determine that this was due to FIDVR, which load models did not have the capability to model.

The inability of static models to capture FIDVR, which left system operators unable to run realistic simulations, led to an increased effort to model load dynamics; the drive for improving models is still present today. Better models were created and occurrences such as FIDVR are able to be modeled in simulation. While this is an important step, the issue of managing FIDVR to ensure system stability still remains. As with other contingencies, effective ways to manage the power system following FIDVR must be investigated and implemented.

1.3 Goals of This Thesis

The goals of this thesis are as follows.

1. Explain the difference in load modeling techniques and show how better models have developed over time.

2. Explain what causes FIDVR and what traditional methods have been used to manage it.

3. Using available software and techniques, create a load model that depicts a power system with parameters that accurately depicts real world conditions.

4. Derive a method to indicate occurrence of FIDVR based on the mathematical foundation of induction motor modeling.

5. Use the derived method to devise a control scheme for mitigating FIDVR and compare it to other methods proposed in research and, in some cases, present in the system already.

The chapters of this thesis are organized as follows.

- Chapter 2 consists of a literature review on load modeling, FIDVR, and FIDVR mitigation methods.

- Chapter 3 discusses the process by which the model was created.

- Chapter 4 investigates induction motor modeling and explains how the technique proposed by this paper is derived.

- Chapter 5 uses the proposed technique in a control scheme and compares it to another control scheme.

- Chapter 6 lists conclusions and possible future work.

Chapter 2

Literature Review

2.1 System Stability

2.1.1 Rotor Angle Stability

As noted in [1], traditional stability problems deal with maintaining the synchronism of a system reliant on synchronous machines to generate power. The behavior of these synchronous machines is dependent on the relationship between mechanical and electrical torque. This relationship is represented by the *swing equation*, which is:

$$J\frac{d\omega_m}{dt} = T_m - T_e \tag{2.1}$$

where J is the moment of inertia, ω_m is the motor angular velocity, t is time, T_m is mechanical torque, and T_e is electrical torque. Often, the swing equation includes a damping factor and is expressed in per unit. This form of the equation can be derived as follows:

$$H = \frac{1}{2} \frac{\omega_{0m}^2}{VA_{base}}$$

$$J = \frac{2H}{\omega_{0m}^2} VA_{base}$$

$$2H \frac{d}{dt} \left(\frac{\omega_m}{\omega_{0m}} \right) = \frac{T_m - T_e}{VA_{base}/\omega_{0m}} \tag{2.2}$$

$$2H \frac{d\bar{\omega}_r}{dt} = \bar{T}_m - \bar{T}_e$$

where variables with a bar represent per unit values. When disturbances occur, the balance of torques in machines change, which causes change in speed and transfer of load between machines [1]. This phenomenon can cause stability issues, and is resolved either through restorative torques or by removing machine(s) from the system for a time. Depending on the seriousness of the disturbance, rotor angle stability can be classified as *small signal stability* for small distrurbances and *transient stability* for larger disturbances.

2.1.2   Voltage Stability

According to [2], voltage stability is "the ability of a power system to maintain steady voltages at all buses in the system after being subjected to a disturbance from a given initial operating condition. It depends on the ability to maintain/restore equilibrium between load demand and load supply from the power system." At the core of maintaining voltage stability is the relationship between power supply and load. Key to maintaining voltage levels is being able to supply the reactive power demands of the system. Following a disturbance in the system, load power is restored through slip adjustment in induction motors, distribution voltage regulators, tap-changing transformers, and thermostats [2]. This can increase reactive power demand in the system, which contributes to reduced voltage levels. This phenomenon is also known as voltage collapse, which is marked by prolonged, reduced voltage levels following a disturbance. If not remedied, voltage collapse can result in significant loss of load and wide spread outages.

The problem of voltage collapse can be further compounded because reactive power does not travel as well as real power, so the ability of the system to provide reactive support is somewhat limited to local resources. When disturbances cause the removal of lines or reactive power sources, this further hampers the system's ability to maintain voltage. While voltage collapse is more common, voltage instability can occur as the result of overvoltage levels as well. According to [2], this is caused by capacitive behavior of the network as well as the inability of the system to operate below a certain level of load.

Voltage stability can also be categorized as *Small Disturbance* and *Large Disturbance* Voltage Stability. Small Disturbance Stability refers to the stability when a system is subjected to small perturbations, like small changes in load, which can be common. Large Disturbance Stability, on the other hand, refers to stability when a system undergoes a significantly more serious event, such as loss of load, lines, or generation.

There are numerous methods used to mitigate voltage stability issues. One of these is the use of FACTS devices, such as SVC and STATCOM. These devices can act as a reactive power source in order to offset an increased reactive power demand. Another method is load shedding, which responds to an increased reactive demand by dropping reactive demand. In addition, other sources of generation may be run in order to provide for the demand of the system.

2.2   Load Modeling

Demand comes from a variety of sources, from residential customers to industrial, and is comprised of a plethora of devices and components. In order to accurately depict the behavior of a power system in studies and simulations, it is imperative to have load models that capture real world behavior. Capturing load behavior can be quite challenging. Resistive loads, such as those in incandescent lighting and resistive

heating that used to be prevalent in system load composition, have very simplistic behavior.

There are much more complex loads present in a power system, such as, motors and electronic loads. The behavior of these types of loads is not as simplistic, and include unique dynamics. The dynamic behavior of these types of loads makes the need for accurate load models even more critical. This chapter presents some load modeling techniques as well as a history of the process by which better load models were obtained.

2.2.1 Static Load Models

Traditionally, load models are classified into two types: *static* and *dynamic* models. Static models, generally the simpler of the two types, represent the load characteristics as an algebraic function of voltage and frequency [1]. They can be expressed with both an exponential model for both real and reactive power. These models are as follows:

$$P = P_0(\bar{V})^a$$
$$Q = Q_0(\bar{V})^b \qquad\qquad (2.3)$$
$$\bar{V} = \frac{V}{V_0}$$

where P is the active power of the load, Q is the reactive power of the load, V is the bus voltage magnitude, and numbers with the subscript $_0$ represent the variable values at initial operating conditions [1]. The exponents a and b adjust the voltage dependency of the load model. For values of 0, 1, and 2, the load models are known as constant power, constant current, and constant impedance, respectively. Generally, active power of loads is represented by a constant current model and reactive power is represented by a constant impedance model [1].

Another method of static load modeling is through use of a polynomial model, which is represented by the following equations:

$$P = P_0(p_1\bar{V}^2 + p_2\bar{V} + p_3)$$
$$Q = Q_0(q_1\bar{V}^2 + q_2\bar{V} + q_3)$$

(2.4)

The coefficients p_1, p_2, and p_3 represent the constant impedance, constant current, and constant power coefficients respectively. The same is true for the q coefficients. Thus, this model allows for constant power, current, and impedance components in one model. The polynomial model is also known as the *ZIP model*, referring to its constant impedance (Z), constant current (I), and constant power (P) parameters. The models can be updated to include a frequency component by multiplying either equation by a factor of

$$1 + K\Delta f$$

(2.5)

As stated, static load models are easier to model than dynamic models, and in some cases are sufficient to model load behavior [3]. However, for some stability studies, the dynamics of various load components can have a considerable effect on system stability. Thus, it is necessary to use the more complex, dynamic load models.

2.2.2 Dynamic Load Models

In cases where static models are not sufficient to capture realistic behavior of the system, dynamic load models must be employed. The term "dynamic load models" encompasses a wide range of different components, each with unique behavior. One type of component critical to dynamic stability studies is the induction motor. Induction motors can comprise from 60 to 70% of total system load [1]. They have a similar behavior to synchronous generators, only the roles of the mechanical and electrical torques are opposite. Thus, the rotor acceleration equation is

$$2H\frac{d\omega_r}{dt} = (T_e - T_m).$$

(2.6)

Other components with unique behavior include some types of lighting and electronic loads. Lighting, such as fluorescent lights, shut of below certain voltage levels and have electronic ballasts [1] [4]. Electronic loads will shut off around 50% of rated voltage, and act as constant real power loads [4]. Dynamic modeling is also necessary to model protective equipment, such as relays, to show behavior when tripped. Different methods of generation, such as wind and solar, also require detailed models to depict behavior. This holds true for many other components present in a power system. The purpose of dynamic modeling is to capture dynamic behavior that cannot be seen with static models. This allows for more realistic simulations and tests.

2.3   Load Modeling History

2.3.1   Need for Improved Models

The improvement of load models has been an ongoing process that has taken place for a number of years. As recently as 1993, IEEE recognized that even the state of the art models of the time needed to be improved. The Task Force on Load Representation for Dynamic Performance noted that overly-optimistic representation could result in system vulnerabilities, while overly-pessimistic representation could lead to wasted expenses to account for system deficiencies that did not actually exist [5]. The report also noted that at the time, 50% of a conducted survey were not satisfied with the load models available.

The Task Force published a follow up to their initial report in 1995. In it, they made recommendations of models to use in a variety of different situations [6]. One suggestion of note involved the different types of load connected to a bus. At the time, "(m)ost dynamic programs allow(ed) multiple generators, multiple motor loads, and a single static load model to be connected to a bus" [6]. The Task Force recommended that multiple types of each individual load be able to be connected to a bus. This

type of load diversity would serve to better represent the load composition present in the real system. This foresight proved to be useful, as modeling load diversity would serve as a driving force and important feature in present-day load modeling innovations.

The shortcomings of load models at the time were highlighted by a number of real world events. In several cases, utilities found that faults that simulations showed would be cleared quickly actually resulted in stability issues and dropped load. The Southern California Edison Company (SCE) experienced numerous issues such as this, and conducted tests to determine the root cause of these issues [7]. They found that the primary cause of these stability issues was the stalling of residential single-phase air conditioners. When voltage at a bus dropped below 60%, the motors would stall, causing bus voltage to delay in recovering to its original level. This phenomenon is known as Fault Induced Delayed Voltage Recovery (FIDVR).

2.3.2 FIDVR

NERC defines FIDVR as "the phenomenon whereby system voltage remains at significantly reduced levels for several seconds after a transmission, subtransmission, or distribution fault has been cleared. Significant load loss due to motor protective device action can result, as can significant loss of generation, with a potential secondary effect of high system voltage due to load loss. A severe event can result in fast voltage collapse [8]."

When faults occur that depress voltage below the stall point of the motors, the system voltage experiences delay in recovery to pre-fault levels. This is caused by the motors drawing an increased reactive power and current during their stalled phase. This continues until the point that motor thermal protection activates and removes the stalled motors from the system [9]. As the motors are tripped, voltage begins to recover, though there may be issues with overshoot if reactive compensation is present [4]. Finally, the motors reconnect and start again. An example of FIDVR
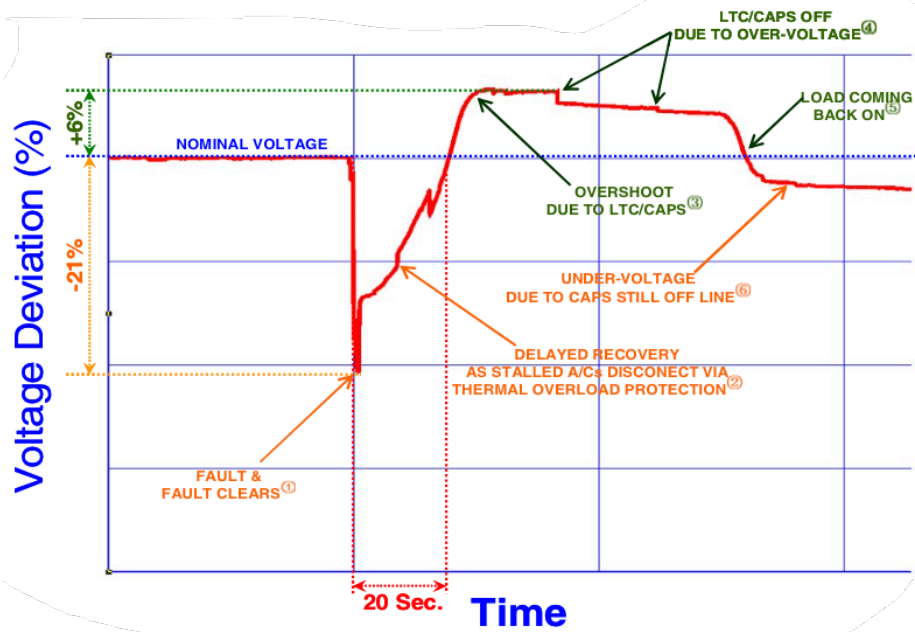
Figure 2.1: Example of FIDVR

from [4] can be found in Fig 2.1. As noted in [7], this is a result of load impedance diminishing and system impedance increasing during these times of faults, which can prevent the necessary reactive power needed for voltage recovery from reaching the loads.

NERC notes that evidence suggests FIDVR events occurred numerous times in the 1970s without the correlation to high A/C motor load being recognized [8]. As seen in SCE's studies, however, the correlation was eventually discovered by multiple parties. On August 22, 1987, the Tennessee Valley Authority (TVA) experienced a significant loss of load, which was eventually traced back to a high A/C load on a hot day [8]. TVA was unable to accurately model the event with the standard load models at the time, just as what SCE experienced. These types of events occurred in multiple locations across the country as well. There were a number of events over a ten year span in Southeast Florida causing significant loss of load that were retroactively determined to have been FIDVR [10]. This study also noted the importance of modeling the distribution system in capturing FIDVR. An FIDVR

event also occurred in the Metro Atlanta area that resulted in the loss of 1900 MW of load and a 15 second voltage recovery time [11].

2.4   Improved Model Development

Events such as those discussed in the previous section and an ever increasing penetration of residential air conditioning into the load profile prompted an increased need for better models. As there were many interested parties, a variety of methods were used. As noted in [7] and [4], SCE used an A/C model that was replaced by a constant impedance when voltage dropped below the stall point. Using this method, they were able to show FIDVR in testing. The Southern Company initially modeled their event using an aggregate load model consisting of a reduced distribution system, 50% small motor penetration, constant current real power model, and constant impedance imaginary power load, which was able to show delayed voltage recovery in simulations [11]. However, they also noted the need to improve their models, as it could only represent one type of induction motor that did not have true stall characteristics. They proposed an improved aggregate load model, seen in Figure 2.2, that would include more motor models to represent different load types, a static load component, and a distribution system model.

The Western Electricity Coordinating Council (WECC), in response to issues with undamped oscillations, also concluded that improved dynamic induction motor models were necessary [12]. Using a single representative motor model and their existing static models, they created an interim load model to "capture the effects" of motor loads on the system [12]. WECC would go on to form a load modeling task force (LMTF) to further efforts into the development of dynamic models. At the time of their progress report in [4], their proposed model included a distribution model, multiple motor models, a model devoted specifically to A/C, and static and electronic load components. Research was done into single phase A/C, specifically the
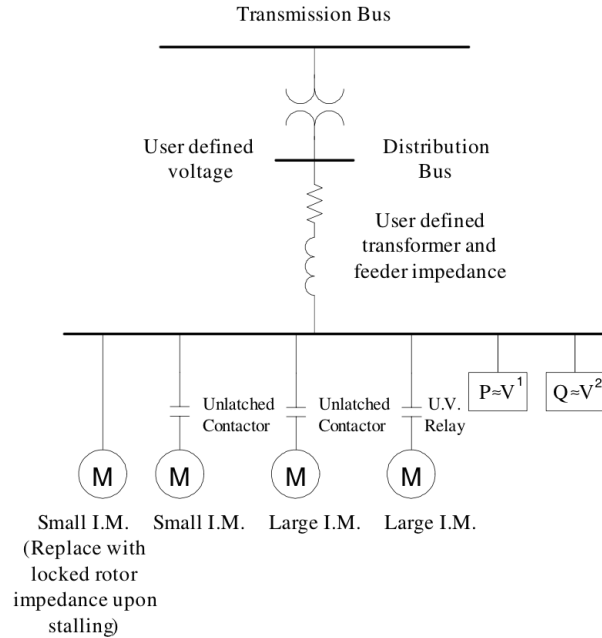
Figure 2.2: Southern Company Proposed Aggregate Model

compressor motor, as WECC concluded that a three phase model could not accurately depict the behavior of single phase motors [4].

As a result of their efforts, the WECC LMTF decided upon a phasor model to represent single phase A/C [13]. Using a phasor representation technique normally used for power electronics, they were able to model behavior observed in their tests. The results of their research yielded the WECC Composite Load Model, which can be seen in Figure 2.3 [14].

The motor types are as follows [15]:

- **Motor A**: Three phase commercial cooling compressor motors

- **Motor B**: Residential and commercial fan motors

- **Motor C**: Direct connected commercial pump motors

- **Motor D**: Single phase residential air conditioning.
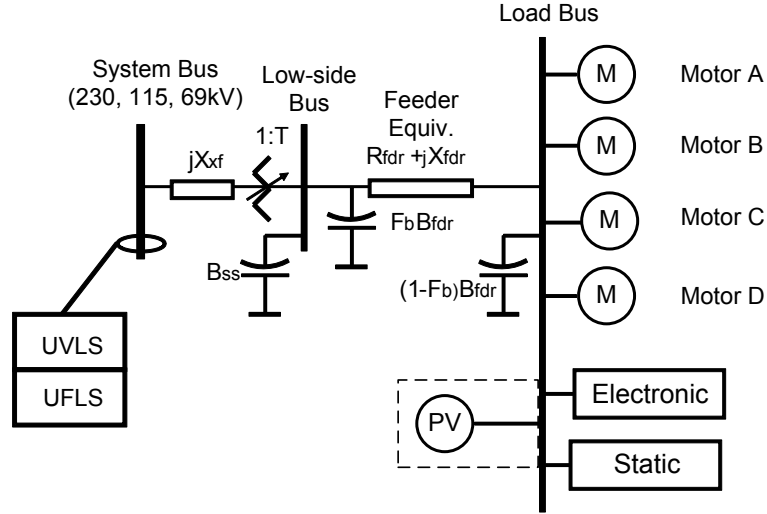
Figure 2.3: WECC Composite Load Model

Today, most commercial dynamic simulation tools include some form or aggregate load model for use in simulations.

2.5 Managing FIDVR

As the penetration of residential A/C load increases, the issue of FIDVR is now more prominent than ever. A considerable amount of research has been done to both study and suggest techniques to manage this phenomenon. Some of this research has led to the setting of benchmarks for voltage recovery, while other parts have led to the proposal of techniques to mitigate the voltage collapse. This section overviews some of the current methodology used to manage FIDVR.

2.5.1 Voltage Recovery Standards

In order to analyze and determine the severity of a voltage drop, there must be a standard for comparison. Peak Reliability set a standard requiring that the voltage dip cannot exceed 20% 30 seconds after the occurrence of a fault [16]. A graph of this standard can be seen in Figure 2.4 [16].

14
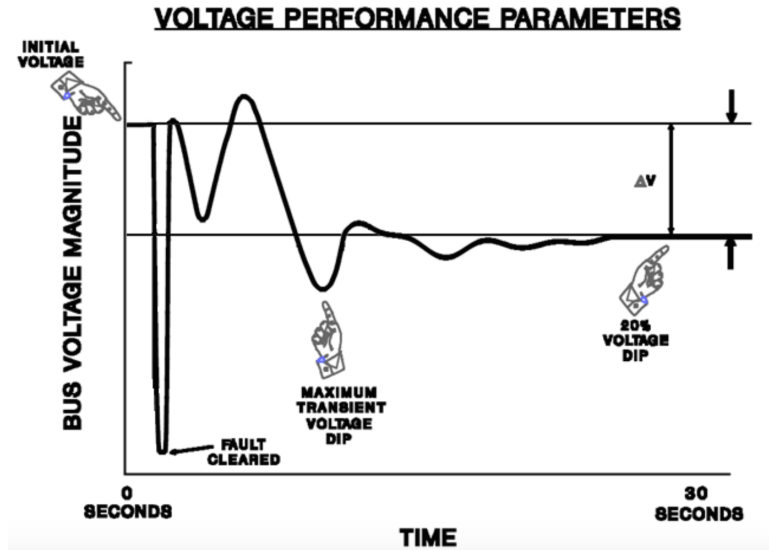
Figure 2.4: Peak Reliability Voltage Recovery Standard

However, some institutions have implemented different recovery standards. PJM created a transient recovery envelope, as seen in Figure 2.5 [17].
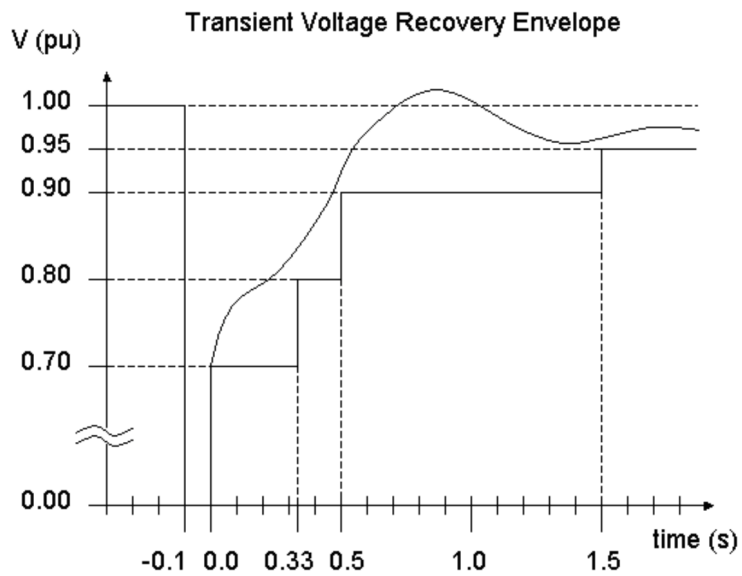
Figure 2.5: PJM Voltage Recovery Standard

This standard requires recovery to 80% of pre-fault voltage within 20 cycles of a fault clearing, and recovery to steady state voltage minimum in 1.5 seconds.

15

Standards such as these are also known as Transient Voltage Recovery Criterion (TVRC) in some literature [18].

2.5.2 Demand Side Solutions

As previously stated, the main issue causing FIDVR is a surge in reactive power demand by the stalling motors. Thus, in order to mitigate the voltage drop, some method of dealing with this increased reactive demand is necessary. While some techniques involve action by the generators or utilities, some solutions can be implemented on the demand side. One such method is under voltage load shedding, or UVLS. This technique will shed a portion of a load at a bus when the voltage remains below a certain level for a certain amount of time. Traditional UVLS sheds the load at the bus in equal proportion, but other methods have been proposed. Some research proposes that using Kinetic Energy measurements to determine the most effective motor loads to drop can be more effective than a traditional scheme [18].

Korea Electric Power Corporation (KEPCO) features a UVLS that sheds predetermined loads following certain contingencies. They modeled a contingency for varying levels of induction motor load and compared voltage recovery first without UVLS then with it implemented; their study showed considerably quicker recovery of voltage to pre-fault levels [19].

While UVLS has been shown to be effective in mitigating FIDVR in some cases, it may not work in some severe events. NERC notes that while UVLS is effective in managing FIDVR and limiting the size of a disturbance, it is not a feasible solution for preventing fast voltage collapse [8]. Thus, individual evaluation must be performed to determine if UVLS is a feasible management technique.

2.5.3 Supply Side Solutions

Another technique used to deal with an increased reactive demand is through supply side reactive compensation. Instead of eliminating some of the demand, this technique instead provides more reactive power for the system to utilize. Reactive compensation can be provided using FACTS devices, such as STATCOM or SVC. Following the FIDVR event experienced by the Southern Company in Atlanta, the Georgia Transmission Company (GTC) installed an SVC in order to prevent any future incidents [20]. It does not provide steady state compensation, but can provide either 130 or 260 MVAR when bus voltage falls bellow a specified threshold; this compensation was designed to meet recovery standards that are consistent with PJM. Another example of an SVC installation to mitigate delayed recovery can be seen in [21].

While reactive compensation has been shown to work, like UVLS in some cases, it may not be effective in situations where there is fast collapse. NERC also notes that while FACTS devices can provide reactive compensation, the most effective manner of supplying more reactive power is through generators [8]. Also, FACTS devices can be expensive to install and maintain. Thus, careful consideration into both performance and cost must be taken when considering this form of supply side solution.

Added transmission capabilities can also reduce vulnerability of a system to delayed recovery events. This can allow greater availability of loads to reactive power sources. However, this method can also cause a voltage drop in a system to spread beyond what it normally would, so application of this technique requires proper investigation and testing [8].

2.5.4 Device Solutions

Some research has been conducted into the effectiveness of implementing FIDVR protection on the device level. In [8], implementation of under voltage protection or improving the design of compressor motors is suggested as effective. Typical

residential A/C devices do not feature under voltage protection, only thermal protection which activates only after the motors stall and draw a high level of current. Research done by Pacific Northwest National Laboratory and SCE has shown that implementing an undervoltage protection tripping when the voltage is below 0.78 pu for a 0.1-0.2 second period was considerably effective in speeding up voltage recovery [22]. Possible issues with device level protection schemes, however, are that there would be a cost associated to install this protection on older equipment, and manufacturers must be convinced to implement it on future models.

Chapter 3

System Modeling

This chapter will discuss and detail the process by which the system model used in this paper was created. The basis of the system model is the 179 Bus model modified by CURENT to model the WECC. A dynamic system model was then applied to this system with parameters based off of real world data obtained through research.

3.1 Modeling Software

In order to properly capture the dynamic behavior of loads in the system model, it is vital to use an appropriate software that has the capability to model dynamics, specifically single phase A/C motors for the purposes of this research. The software also needs to have the capability to observe and analyze the transient response of the system to faults introduced to the system. With this criteria in mind, the software used for all transient analysis in this paper is $DSATools^{TM}$ from *Powertech*. This software comes with a variety of tools that can be used for different applications of power system analysis. The primary tools used in this research were *TSAT* (which allowed for the dynamic load modeling of the system as well as transient contingency analysis), *PSAT* (which calculated the base powerflow solution of the system), and *DSA Output Analysis* (which allows a variety of output parameters to be observed and exported.
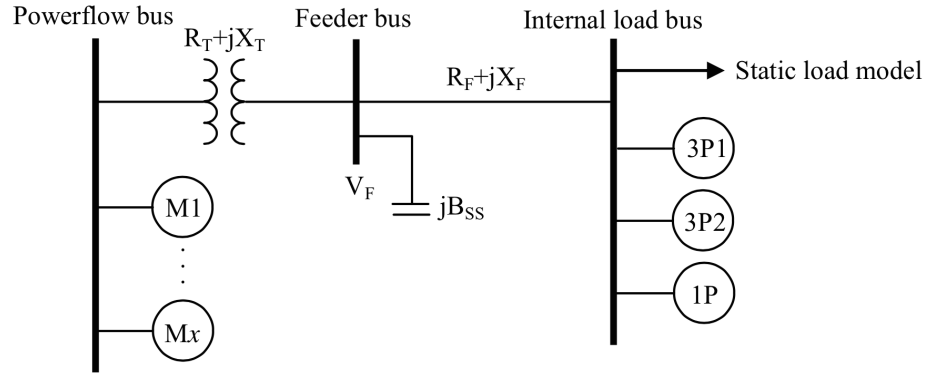
Figure 3.1: TSAT Load Model

As mentioned, the load model of TSAT is vital to this research; it not only must have dynamic models of the individual load components, but it must also be able to assign an aggregate load model composed of different components to the loads in the system. The load model used in TSAT can be seen in Fig. 3.1 [23].

As can be seen, this load model is somewhat similar to the WECC Composite Load Model discussed in Chapter 2. It includes a model for an internal transformer and distribution system, which is critical to modeling events such as FIDVR accurately. This composite load model includes a static load component, two three phase motor load components, and a single phase motor component, which is used to model residential A/C. Within the static load model are components for constant power, constant current, and constant impedance static load, as well as a discharge lighting component, thus allowing the capability to model a diverse static load at each load bus. However, the TSAT load model only allows for the modeling of three different motor loads, as opposed to WECC Composite Load Model, which can model four. Thus, for this application, only three of the four motor types are modeled. The specifics and reasoning of the motor modeling used in this research will be discussed in subsequent sections. Most importantly, the TSAT load model can depict the behavior of residential A/C, which is the driving force behind FIDVR. As such, TSAT was determined to be sufficient to model the behavior necessary to this research. Despite

the inability to model all WECC motor types, this comes with the benefit of reducing the amount of input parameters in the load model, with the WECC model requiring significantly more parameters than TSAT's.

3.2   Component Modeling

This section will describe how the individual components of the aggregate load model are modeled. In all cases, this thesis refers to data taken from WECC; this data was obtained at [24]. The WECC LMTF has both load composition and component parameter data available for use in simulations. So not only is this data realistic, but also based on WECC data, which is the area that is modeled in this paper. Thus, all parameters and composition percentages, unless otherwise specified, will be based on this data.

3.2.1   Single Phase A/C Modeling

Having accurate parameters for residential A/C motors is vital to performing accurate studies and depicting realistic behavior in the system. The need for this type of accurate model is what led the WECC to develop an A/C model that would make studies better depict real world behavior of the motors. The final test report of their motor model, LD1PAC, can be seen in [25]. This report explains what each different parameter is, along with describing the testing process and a range of typical values. There are numerous parameters that depict dynamic behavior in a way a static model cannot, such as the stalling parameters and motor restart parameters. While this research does not use the WECC's Composite Load Model, the parameters given in the report are the same in TSAT's A/C model. The values for the parameters were taken from the WECC motor parameter data available. A table of the parameter values used for A/C modeling can be seen in Appendix A.1.

3.2.2 Three Phase Motor Modeling

In addition to A/C motors, there are other, three phase motors that comprise the system load profile. As previously mentioned, the WECC Composite Load Model models three types of three phase motors, named Motors A, B, and C, each representing a different type of motor. However, as TSAT's load model only has the capability to model two three phase motors, for the purposes of this research, only Motors A and B were modeled at load buses, and the Motor C percentage was added to the static load percentage. Again, this simplification was made because the A/C motors drive the behavior studied in this paper, so modeling two three phase motor types was determined to represent a sufficiently diverse load profile. The parameters for Motors A and B can be seen in Appendix A.2 and A.3, respectively, and the values are again taken from WECC motor parameter data.

Note that WECC and TSAT differ in how they handle undervoltage protection of three phase motors. While both have the capability to model this protection and the ability to restart, WECC models that it occurs in two stages based on two separate thresholds as opposed to TSAT modeling that it occurs in one. Thus, rather than be optimistic and model that all of the restarting motors restart at the same time, the decision was made to not model undervoltage protection on the three phase motor models at all. While this does give a pessimistic response of the system, this is preferable to an optimistic assessment, which could lead to unforeseen issues. Again, the component most affecting the desired behavior in this research is not the three phase motors, but the A/C motors.

3.2.3 Static Load Modeling

The static load component of TSAT's load model has percentages for all three basic types of static load: constant power, constant current, and constant impedance. In addition, it has a percentage for discharge lighting load. Based on convention, such as that used in [10], the real static load is modeled in this system as constant current

and imaginary static load is modeled as constant impedance. The total percentage of load composition of the individual load components must add up to 100%. Thus, static load percentage in this system is assigned as the percentage remaining after the motor load percentages are assigned. WECC does have a load component for electronic load, so the electronic load percentage in their load composition data is modeled as the discharge lighting load in this system. The frequency dependent characteristics of the load is not modeled as this research deals with voltage stability.

3.3   Test System

The test system used in this research is the 179 Bus system modeling the WECC. A bus drawing of this system can be seen in Fig. 3.2 [26]. The model obtained from CURENT included some dynamic data, such as generator and exciter models, but all of the loads present in the system were modeled as static load. Thus, the TSAT load model is applied to a majority of the load buses in the system. Some load buses in the system, however, have negative real loads; this is done to represent net generation at certain buses where a generator model would not be appropriate. As the TSAT load model is percentage based (percent of the total load is assigned to the load components), it is not possible to model both a negative net load and a separate motor load at the bus. Thus, the loads at buses with negative real power are modeled with a constant current static load.

3.3.1   Load Composition

Once the load models were assigned to the appropriate buses, the load composition percentages need to be applied. The WECC load data mentioned earlier, [24], included load composition data based on geographical area, season, and time of day. The WECC is broken down into climate zones, each with a different load profile. A map of these geographical areas can be seen in Fig. 3.3 [27].
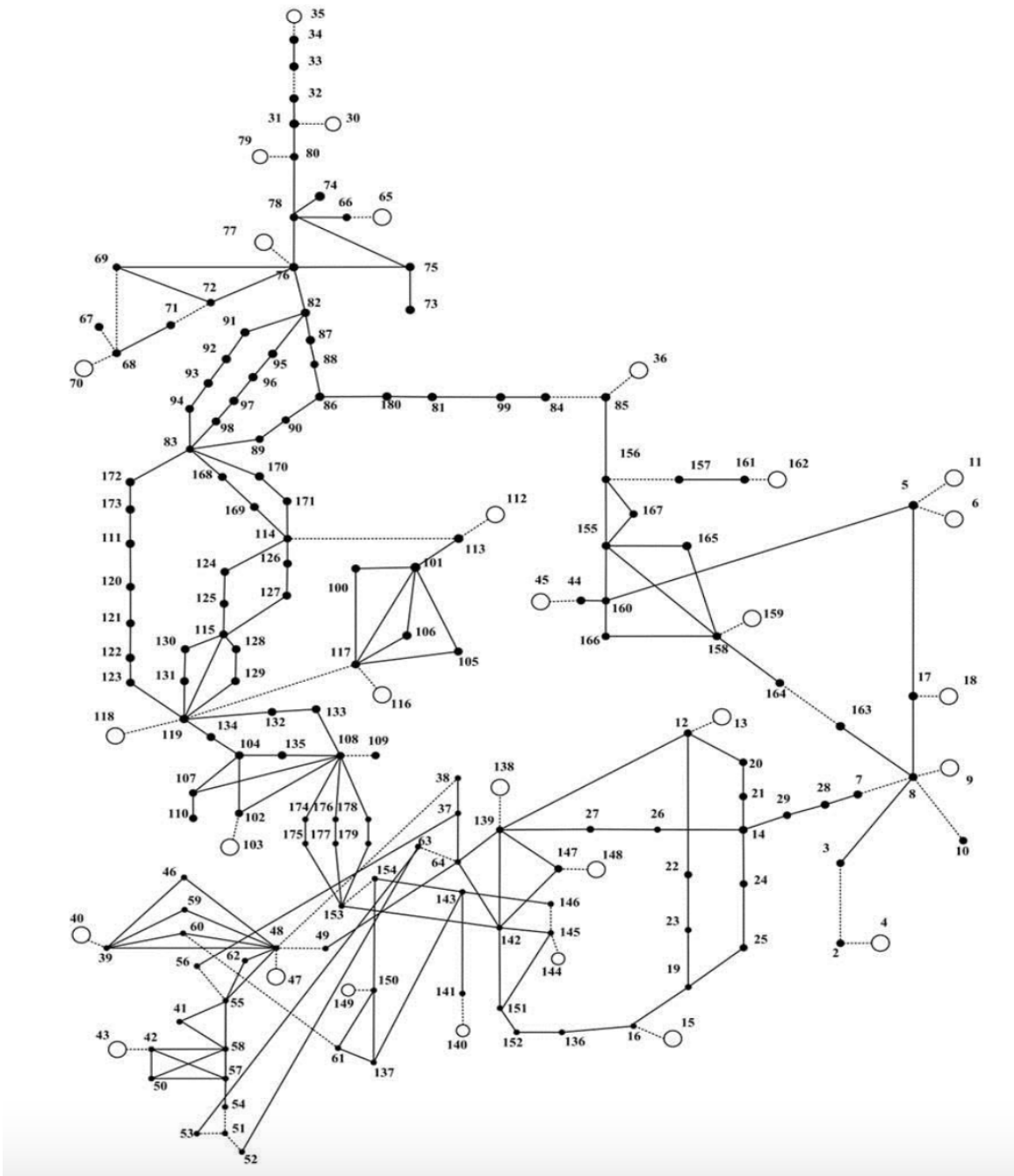
Figure 3.2: WECC 179 Bus System

NWC – Northwest coast
NWV – Northwest valley
NWI – Northwest inland
RMN – Rocky mountain
NCC – N. Calif. coast
NCV – N. Calif. Valley
NCI – N. Calif. Inland
HID – High desert
SCC – S. Calif. coast
SCV – S. Calif. Valley
SCI – S. Calif. Inland
DSW – Desert southwest
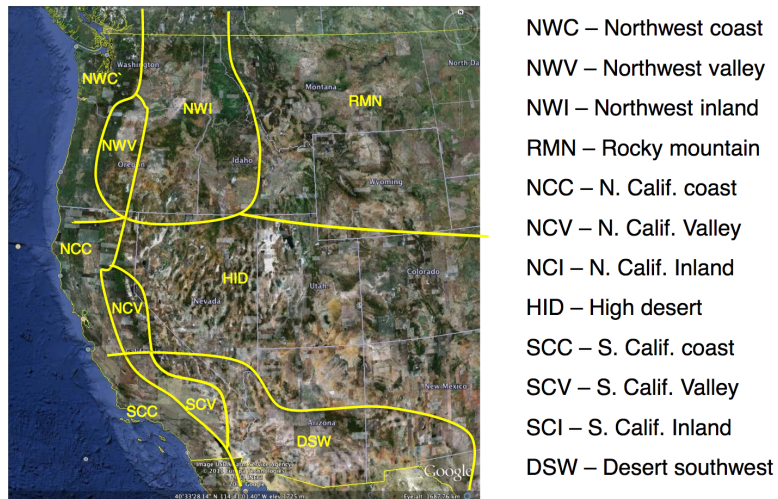
Figure 3.3: WECC Climate Zones

The western United States has diverse geography, and as such the load composition will be different among these zones. In addition, WECC data includes different load composition for the type of load in each of the areas. These include types such as commercial, residential, mixed, and rural. Each of these types has different load components and percentages. In order to apply this type of load diversity to the system in this research, the names of the buses were used in conjunction with WECC load composition data to place the buses geographically where possible, and from this the system was divided into areas. Table 3.1 lists the different areas and load types associated with the load buses in the system.

As the 179 bus system is an aggregation of the actual system (each bus represents an aggregation of numerous actual system buses), the majority of buses are represented with the Mixed load type. The exception to this is for buses with a name and voltage level exactly matching a bus in the WECC data, in which case it is represented as the load type in the WECC data. Thus, there are some residential and rural/agricultural load types in the system. This provides the benefit of greater load diversity in the system. The PPA_AUX loads model exclusively generator buses that do not have bus names consistent with names present in WECC data that indicate a different load type.

Table 3.1: 179 Bus Load Bus Climate Areas and Load Types

179 Bus Load Bus Climate Areas and Load Types		
Climate Zone	Load Type	Buses
NWC	Mixed	31, 34, 67, 71
NWC	Residential	80
NWV	Mixed	119
NWI	Mixed	78
NWI	Rural/Ag.	76, 77
RMN	Mixed	11, 66, 75, 85, 156, 157, 161
NCC	Mixed	102, 104, 107, 110
NCV	Mixed	106, 117
HID	Mixed	5, 17, 44, 101, 105, 108, 109, 113, 139, 155, 158, 164, 165, 166, 167
HID	Residential	138
SCC	Mixed	41, 50, 51, 54, 55, 57, 58, 59, 62
SCV	Mixed	142, 144, 145, 151, 152
SCI	Mixed	48, 61, 137, 140, 141, 143, 154
DSW	Mixed	2, 8, 10, 12, 16, 19, 136
PPA_AUX	N/A	4, 6, 9, 13, 15, 18, 30, 35, 36, 40, 43, 45, 47, 65, 70, 79, 103, 112, 116, 118, 148, 149, 159, 162

As important as it is to model the climate zone and load type, it is also important to model season and time of day. For example, A/C load percentage will be drastically different for a summer month in the middle of the day and for a winter month when it is significantly cooler. The WECC has load composition data available for a number of seasons and times. As previously mentioned, FIDVR has been linked to high penetration of residential A/C; for this reason, the primary load case used in fault analysis in this research is HS18, or High Summer, Hour 18. This case has many load types with significant A/C percentages, so it is ideal for performing tests involving FIDVR. The load composition for this case can be seen in Appendix B.1.

In addition, a system model for HW08, or High Winter, Hour 08 is used for a seasonal analysis in Chapter 5. The load composition for this case can be seen in Appendix B.2. Each fault analysis will explicitly state the load case used in simulation.

3.4   System Model Validation

This section describes testing done to ensure that the 179 bus model used in this research is valid and exhibits realistic behavior.

3.4.1   Static-Dynamic Load Model Comparison

The first test performed was to compare the original static load model response to a fault to that of the dynamic model with WECC data. Using TSAT's N-1 Contingency feature, a series of system wide bus faults were simulated with both the static load model and HS18 model. There was a stark difference in the behavior of the system for a good number of the faults. One example is for a bus fault at Bus 7. At 1 second there is a three phase bus fault, which is cleared after 5 cycles and Line 7-8 is removed. The static model showed almost no delay in voltage recovery in the system,

while the HS18 case showed a noticeable delayed voltage recovery. The two responses are compared in Fig. 3.4.

(a) Static Load Model

(b) HS18 Load Model
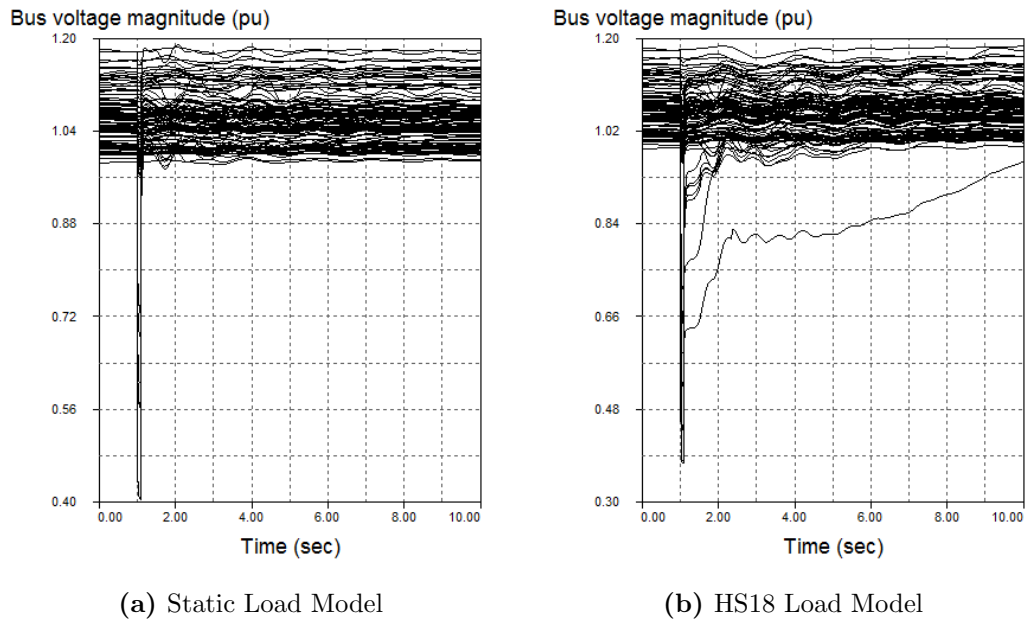
Figure 3.4: Load Model Comparison, Bus 7 Fault

The importance of dynamic models is evident from this test, as a static model indicates that the system would recover in a short amount of time, which is in stark contrast to the dynamic model. Through this test it is seen that the dynamic model used in this research is capable of capturing the FIDVR phenomenon.

3.4.2 Frequency Response Test

While the research in this thesis deals with voltage response, it is still important to show that the frequency response of the system is realistic in order to ensure validity. Thus, a simulation of generation loss at Bus 138 was run to see if the frequency would drop as it should. This test was run for three load models: static, HS18, and HW08. The frequency responses of all three models to this contingency are compared in Fig. 3.5.

28
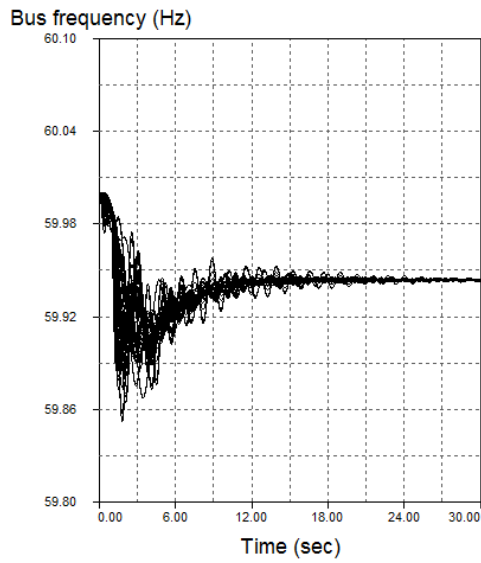
(a) Static Load Model
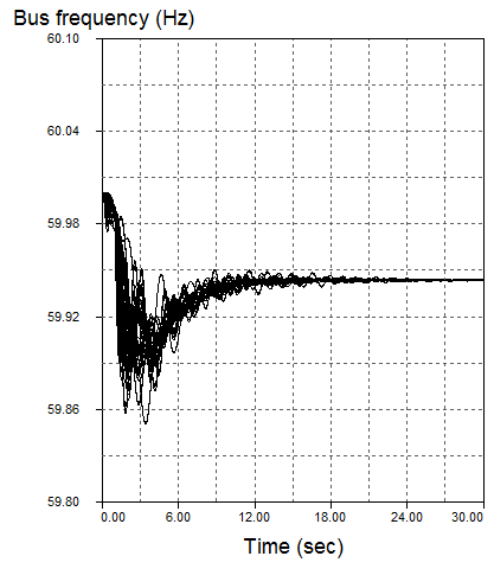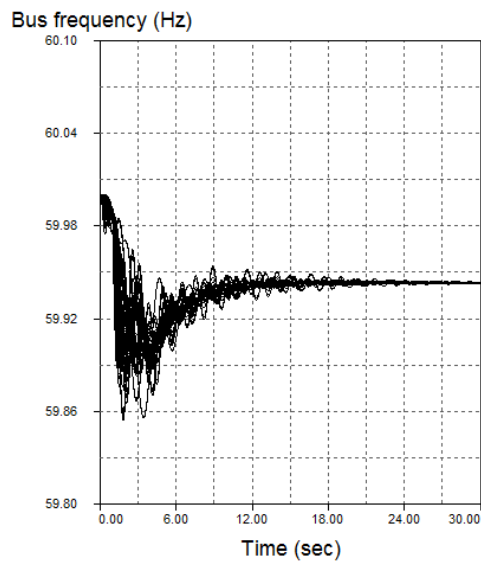
(b) HS18 Load Model

(c) HSW08 Load Model

Figure 3.5: Frequency Response Comparison, Generator 138 Disconnect

In all three cases, the frequency response is similar; the system frequency decreases in response to the loss of generation, before settling at a slightly lower frequency after, as was expected. These are similar to reported responses in the literature for the WECC. Thus it can be seen that the load models used in this research exhibit appropriate, realistic behavior and provide an accurate representation of the faults analyzed.

Chapter 4

Induction Motor Behavior

This chapter discusses modeling techniques for induction motors. As motors, specifically residential A/C motors, are the driving force behind FIDVR, it is important to model them accurately. From the modeling techniques discussed, a method of indicating the occurrence of FIDVR in motors is proposed.

4.1 Induction Motor Modeling

As indiction motors comprise a significant percentage of the overall load profile in a power system, it is vital to model them accurately. Induction motors consist of two elements: the armature and the field [1]. As is typically the standard, this paper refers to the armature as the stator and the field as the rotor. Both the stator and rotor windings produce magnetic fields. At no load, the fields rotate at the same speed; because of this the rotor voltages and currents are approximately zero. As load is applied, however, the rotor speed will decrease, thus causing what is known as slip, which is the positive torque needed to power the load. The speed and slip equations of induction motors are given by

$$n_s = \frac{120 f_s}{p_f}$$

$$s = \frac{n_s - n_r}{n_s} \tag{4.1}$$

where n represents speed, f represents frequency, p_f is the number of poles, s is slip, and subscripts $_s$ and $_r$ represent stator and rotor, respectively. Fig. 4.1 shows a representation of the stator and rotor circuits in an induction machine [1].
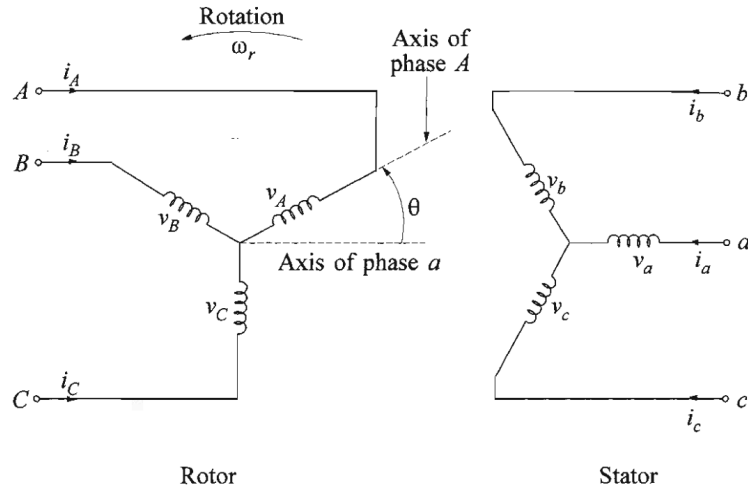
Figure 4.1: Induction Motor Circuits

θ is the angle that rotor phase A leads stator phase a by; it is given by the equations

$$\theta = \omega_r t$$

$$\theta = (1 - s)\omega_s t \tag{4.2}$$

where ω represents angular velocity. The voltage and current equations of the stator and rotor are given as follows:

$$v_a = \frac{d}{dt}\psi_a + R_s i_a$$
$$v_b = \frac{d}{dt}\psi_b + R_s i_b$$
$$v_c = \frac{d}{dt}\psi_c + R_s i_c \qquad (4.3)$$
$$i_a + i_b + i_c = 0$$

$$v_A = \frac{d}{dt}\psi_A + R_r i_A$$
$$v_B = \frac{d}{dt}\psi_B + R_r i_B$$
$$v_C = \frac{d}{dt}\psi_C + R_r i_C \qquad (4.4)$$
$$i_A + i_B + i_C = 0$$

where ψ is the flux linkage, R is phase resistance, and the subscripts represent the phase of the stator or rotor. The flux linkage is effected by numerous inductances in the circuit, which are dependent on both angle and time. However, induction motor models can be simplified through use of the dq0 transformation.

The dq0 transformation takes advantage of the fact that for balanced operation, the mmf wave due to stator currents in an induction motor is stationary with respect to the rotor [1].Thus, the sinusoidal mmf wave is represented as two sinusoidal waves each peaking over different axes, the d and q axes. The stator parameters expressed in the dq0 reference frame are:

$$i_{ds} = \frac{2}{3}[i_a \cos \omega_s t + i_b \cos \omega_s t - 120° + i_c \cos \omega_s t + 120°]$$
$$i_{qs} = \frac{-2}{3}[i_a \sin \omega_s t + i_b \sin(\omega_s t - 120°) + i_c \sin(\omega_s t + 120°)]$$
$$\psi_{ds} = L_{ss}i_{ds} + L_m i_{dr}$$
$$\psi_{qs} = L_{ss}i_{qs} + L_m i_{qr} \qquad (4.5)$$
$$v_{ds} = R_s i_{ds} - \omega_s \psi_{qs} + \frac{d\psi_{ds}}{dt}$$
$$v_{qs} = R_s i_{qs} - \omega_s \psi_{ds} + \frac{d\psi_{qs}}{dt}$$

The rotor parameter equations expressed in the dq0 reference frame are:

$$\frac{d\theta_r}{dt} = s\omega_s$$

$$i_{dr} = \frac{2}{3}[i_A \cos\theta_r + i_B \cos(\theta_r - 120°) + i_C \cos(\theta_r + 120°)]$$

$$i_{qr} = -\frac{2}{3}[i_A \sin\theta_r + i_B \sin(\theta_r - 120°) + i_C \sin(\theta_r + 120°)]$$

$$\psi_{dr} = L_{rr}i_{dr} + L_m i_{ds} \qquad (4.6)$$

$$\psi_{qr} = L_{rr}i_{qr} + L_m i_{qs}$$

$$v_{dr} = R_r i_{dr} - \frac{d\theta_r}{dt}\psi_{qr} + \frac{d\psi_{dr}}{dt}$$

$$v_{qr} = R_r i_{qr} + \frac{d\theta_r}{dt}\psi_{dr} + \frac{d\psi_{qr}}{dt}$$

where θ_r is the angle that the d axis leads rotor phase A by and the inductance parameters are given by the equations:

$$L_m = \frac{3L_{aA}}{2}$$

$$L_{ss} = L_{aa} - L_{ab} \qquad (4.7)$$

$$L_{rr} = L_{AA} - L_{AB}.$$

4.2 Steady State Motor Modeling

Using the modeling techniques discussed in the previous section, it is possible to create a steady state model for induction motors. Based on the dq0 transformation, the stator current can be described using the following equations:

$$i_s = i_{ds}\cos\omega_s t - i_{qs}\sin\omega_s t$$

$$i_s = i_{ds}\cos\omega_s t - i_{qs}\cos(\omega_s t + 90°)$$

$$\bar{I}_s = I_{ds} + jI_{qs} \qquad (4.8)$$

$$I_{ds} = \frac{i_{ds}}{\sqrt{2}}, I_{qs} = \frac{i_{qs}}{\sqrt{2}}$$

where $\bar{I}_s$ is the RMS stator current phasor. The stator voltage is given by

$$\bar{V}_s = V_{ds} + jV_{qs}$$

$$V_{ds} = \frac{v_{ds}}{\sqrt{2}}, V_{qs} = \frac{v_{qs}}{\sqrt{2}}.$$

(4.9)

Under steady state, all time derivatives are equal to zero, and thus drop out of the equations. Substituting the stator flux linkage equations into the stator voltage equations given in Equation 4.5, the following equations are obtained:

$$v_{ds} = R_s i_{ds} - \omega_s L_{ss} i_{qs} + L_m i_{qr}$$

$$v_{qs} = R_s i_{qs} + \omega_s L_{ss} i_{ds} + L_m i_{dr}$$

(4.10)

Further substitution yields:

$$\bar{V}_s = R_s \bar{I}_s + j\omega_s L_{ss} \bar{I}_s + j\omega_s L_m \bar{I}_r$$

$$= R_s \bar{I}_s + j\omega_s (L_{ss} - L_m) \bar{I}_s + j\omega_s L_m (\bar{I}_s + \bar{I}_r)$$

$$= R_s \bar{I}_s + jX_s \bar{I}_s + jX_m (\bar{I}_s + \bar{I}_r)$$

(4.11)

with

$$X_s = \omega_s (L_{ss} - L_m)$$

$$X_m = \omega_s L_m$$

$$\bar{I}_r = I_{dr} + jI_{qr}$$

$$I_{dr} = \frac{i_{dr}}{\sqrt{2}}, I_{qr} = \frac{i_{qr}}{\sqrt{2}}$$

(4.12)

X_s represents the stator leakage reactance and X_m represents the magnetizing reactance. The rotor voltage equations are then given by

$$v_{dr} = R_r i_{dr} - s\omega_s (L_{rr} i_{qr} + L_m i_{qs})$$

$$v_{qr} = R_r i_{qr} + s\omega_s (L_{rr} i_{dr} + L_m i_{ds})$$

(4.13)

Note that when the rotor circuits are short circuited, $v_{dr} = 0$ and $v_{qr} = 0$. The phasor value of the rotor current is then given by

35

$$\bar{V}_r = 0 = \frac{R_r}{s}\bar{I}_r + j\omega_s L_{rr}\bar{I}_r + j\omega_s L_m \bar{I}_s$$

$$= \frac{R_r}{s}\bar{I}_r + jX_r\bar{I}_r + jX_m(\bar{I}_s + \bar{I}_s) \tag{4.14}$$

X_r represents the rotor leakage reactance, and is given by

$$X_r = \omega_s(L_{rr} - L_m) \tag{4.15}$$

Using the derived equations, a steady state model for an induction motor is obtained. This model can be seen in Fig. 4.2 [1]. Note that the model has all values referred to the stator side.
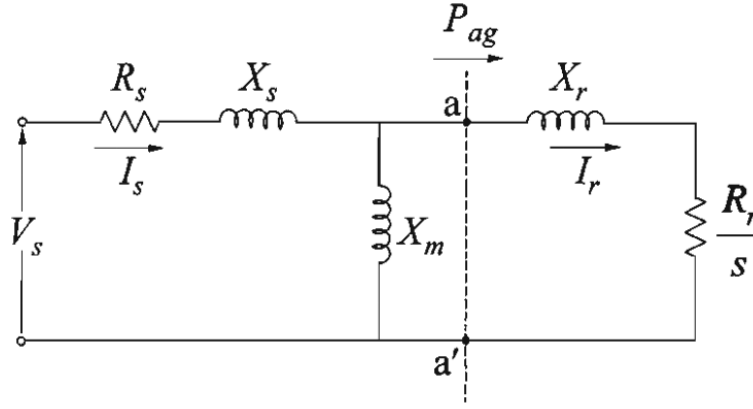
Figure 4.2: Induction Motor Steady State Model

4.3 FIDVR Effect on Motor Model

In order to determine if a motor is experiencing FIDVR, it is important to look at the possible effects that FIDVR has that would be reflected in the model. One issue is that following a fault, there can be dynamics at play that cannot be as easily modeled or represented with the steady state model derived in the previous section. According to Kundur, for applications with small motors, the rotor-circuit dynamics are fast enough that they need not be accounted for precisely; because of this simplification the induction motor can be represented with the steady state equivalent [1]. Thus,

as the residential air conditioners are smaller motors, this assumption is made for this paper and the steady state model is used to derive the proposed methodology for identifying FIDVR. Using the same simplification as in [18], which assumes that $X_m \gg X_s$ and R_s is negligible, the steady state model in Fig. 4.2 is simplified to that seen in Fig. 4.3.
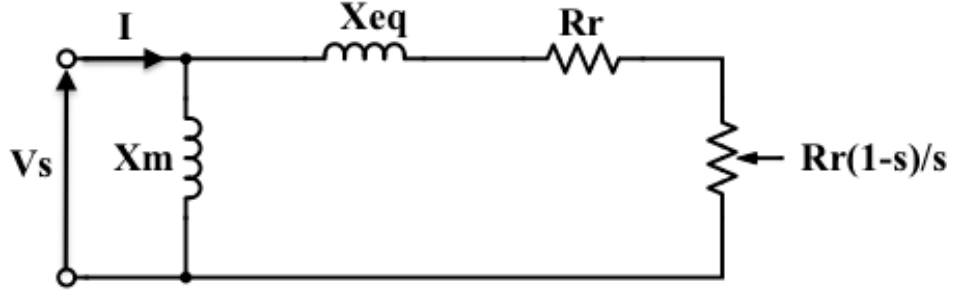
Figure 4.3: Simplified Induction Motor Steady State Model

In the figure above, $X_{eq} = X_s + X_r$. From this model, it can be seen that the total impedance of the induction motor is equal to

$$\bar{Z}_t = X_m \parallel (\frac{R_r}{s} + jX_{eq}) \tag{4.16}$$

and that the relationship between the total impedance of the motor and its voltage and current is

$$\bar{Z}_t = \frac{\bar{V}_s}{\bar{I}} \tag{4.17}$$

Using the same assumption from [18] that $X_m \gg X_{eq}$, Equation 4.16 can be simplified to

$$\bar{Z}_t \simeq (\frac{R_r}{s} + jX_{eq}) \tag{4.18}$$

Now that the steady state model is simplified to this point, it is important to identify the characteristics of an FIDVR event in order to predict what parameters will be impacted. The most apparent physical characteristic of an FIDVR event is

37

that the motors stall after a fault. The stalling causes a significantly reduced motor speed. Based on the slip equation for induction motors

$$\omega = (1 - s)\omega_s \tag{4.19}$$

where ω is the induction motor speed, it can be inferred that a reduction in motor speed is the result/correlates to an increase in slip. Based on Equation 4.18, an increase in slip due to an FIDVR event would lead to a reduction in the $Re\{\bar{Z}_t\}$, as it depends on the slip value. Thus, it can be determined that an FIDVR event will cause a decrease in the real part of the total load impedance of an induction motor, which is a measurable quantity that could be used as an indicator. More, as the A/C motors have low inertia, and are thus classified as "prone-to-stall" [7], this effect should be observable very shortly after a fault.

4.3.1 Proposed Technique

Based on the derivations of this section, this thesis proposes that load impedance be used as an indicator for FIDVR events. However, it is not as simple as measuring the load impedance at all residential air conditioners in the system; these measurements are not available, and also not feasible as it would take a considerable amount of data and equipment installation. Thus using a technique similar to that used in [18], the whole load at a bus will be treated as a single induction motor, as the total load voltage and current at a bus is a much more feasible measurement expectation. The justification for this technique is that FIDVR events typically occur only when residential A/C motor comprise a significant percentage of the total load profile; when this is the case, the dominant behavior of a dominant portion of the load profile should be prevalent. As mentioned, one benefit of the proposed technique is that it significantly reduces the amount of measurements required to be taken as opposed to measuring every single A/C motor.

4.3.2 Impedance Calculation

Using Equation 4.17 to calculate $\bar{Z}_t$, the phasor values of $\bar{V}_s$ and $\bar{I}$ must be known. This requires knowing not just the magnitude of the load voltage and current, but their relative angles. While in some power systems the angle measurements may be readily available, a further simplification in measurements is taken here. Instead of calculating the full phasor value of $\bar{Z}_t$, the magnitude $||\bar{Z}_t||$ is used. This requires taking only the magnitudes of the load voltage and current, $||V_s||$ and $||I||$, respectively. As the magnitude of the load impedance is given by

$$||\bar{Z}_t||^2 = \sqrt{(\frac{R_r}{s})^2 + X_{eq}^2} \tag{4.20}$$

The reduction of the real part of the impedance due to an increase in slip will have a noticeable effect on the load voltage magnitude. The change in the load impedance magnitude calculated in this paper is from this point known as Z Deviation. Z Deviation will represent the change in load impedance at a bus before a contingency and after. The load impedance magnitudes used in testing will be calculated at each of the load buses using the total load voltage and current magnitude measurements. This thesis proposes that for a fault in a system with significant A/C penetration to cause an FIDVR event, there will be a significant Z Deviation at the buses experiencing delayed voltage recovery. Chapter 5 will discuss the details of how and when Z Deviation is calculated in further detail. In addition, Chapter 5 will also investigate the use of Z Deviation in a control scheme used to improve system voltage recovery.

Chapter 5

Implementing Z Deviation Based Control

The goal of this chapter is to compare the effectiveness of mitigating FIDVR by two techniques: a demand side control scheme based around Z Deviation levels and device level undervoltage relays on the single phase A/C motors. These techniques will be compared in three separate cases, each being a line fault located 25% down the length of the line from the first listed bus. In all cases, the fault occurs at 1 second and is cleared after 5 cycles. The faults will be in different locations and show both unique behavior and how FIDVR can be a non-local issue. A case without any form of control or protection will be looked at first in each case to show the worst case scenario and showcase the effects that protection can have.

5.1 Control Schemes

5.1.1 Device Level Protection

Device level undervoltage relay, referred to as UVR, was selected as the control method to compare to the Z Deviation method. This assumes it is much more effective in mitigating FIDVR than a scheme such as traditional undervoltage load shedding.

Traditional load shedding sheds an equal proportion of the programmed load across the load components, whereas UVR sheds only the single phase A/C load. The level of UVR used in each different case is 30%, and the UVR will be present in all motors system wide. This percentage of motor load with UVR would be optimistic by real world standards; the WECC motor model data sheet used in this paper lists a UVR percentage (fuvr) of 10%. However, the goal of this chapter is to compare the effectiveness in identifying and shedding problem load, so while optimistic, it does not interfere with the analysis. Also for the Z Deviation based control scheme, no UVR will be present in any motors during simulation. This is a pessimistic case, but again, the purpose of this chapter is to compare two differing methods of removing problem load. TSAT settings do not base UVR tripping based on percentage of voltage, but instead activate when the voltage at the bus falls below a certain level. For testing purposes, this level has been set at 0.8 pu, with the idea that this would provide similar response to suggested UVR parameters seen in [22]. UVR will trip after 0.2 seconds below this level, which falls within the 6-15 cycle (0.1 to 0.25 second) range given.

5.1.2   Z Deviation Control Scheme

The Z Deviation based demand side control, referred to here as Z Deviation Control, will remove load based on the measured Z Deviation, with load being shed from the buses with the highest Z Deviation. The logic behind the buses at which load is removed will be explained in each different case, and will be based on a threshold chosen in relation to each individual case. Z Deviation used in this method will be calculated as follows:

$$
\begin{aligned}
Z_{m0} &= \frac{V_{m0}}{I_{m0}} \\
ZD &= \frac{Z_{m0} - Z_{m1}}{Z_{m0}}
\end{aligned}
\tag{5.1}
$$

where V_{m0}, I_{ms0}, and Z_{m0} are the average pre-fault magnitudes of load voltage, load current, and load impedance, respectively and Z_{m1} is the average post fault load impedance magnitude used to calculate the Z Deviation. Z_{m1} is calculated as the average of the load impedance from approximately 0.2 seconds following the fault to approximately 0.5 seconds following the fault. This method of calculation was done for multiple reasons: taking a single measurement would increase the risk of a faulty measurement via noise or other reasons, an average better captures any dynamics still in play following the fault, and this type of demand side control would take longer than a method such as UVR, which activates based on going past a threshold. For comparison, the percentage dropped at each bus via this method will equal the percentage of A/C motors with UVR in the corresponding test for each case. This is to fairly compare the effectiveness of the two methods in identifying and removing problem load.

5.2 Defining FIDVR and Recovery Standards

A consistent definition of FIDVR and realistic recovery standards for recovery methods is needed. While FIDVR is clearly defined in the literature, the performance requirements can vary between organizations. For the faults analyzed, it is visually noticeable that the voltage recovery is delayed in the base cases, however it is important to define a threshold. As seen in the WECC "finger diagram" shown in Chapter 2, the standard for recovery following a fault in the WECC is to 80% of pre-fault level within 30 seconds [16]. This standard is fairly loose, and easily met by all of the cases in this thesis, especially following the thermal trip of 80% of the A/C at buses with stalled motors. Critical to voltage recovery in stability, however, is rapid voltage recovery. As such, the methods used in this research focuses on the short term recovery of bus voltage. For this reason, an FIDVR event is defined in this paper as *a fault that results in at least 1 bus with a voltage drop greater than 20% 2 seconds post fault*, or at 3 seconds in the simulations of the cases discussed below. All

three base cases in this paper meet this criteria. The control methods used to aid in voltage recovery will be analyzed at a point that the voltage recovery has exceeded 80% pre-fault levels at all load buses, and in each case this is within 10 seconds. This shorter timeframe was chosen to focus on short term voltage recovery.

5.3   Fault Analysis

Fault analysis in this chapter consists of running simulations for three different lines faults in the 179 bus system. In each case, the line fault occurs 25% down the length of the line from the first bus listed. The three faults are from Bus 37 to 64, Bus 108 to 133, and Bus 14 to 26, In each case, the fault is analyzed using the HS18 based load model with no protection present in the system, and the Z Deviations at 1.5 seconds, or the measurement point for Z Deviation Control, will be listed. Then both UVR and Z Deviation Control are implemented and the recovery rates compared.

5.3.1   37-64 Fault

The fault from Bus 37-64 occurs near a concentration of buses with a high level of A/C, including HID region modeled buses in the near vicinity. This fault results in significant delay in system bus voltage recovery, as seen in Fig. 5.1.
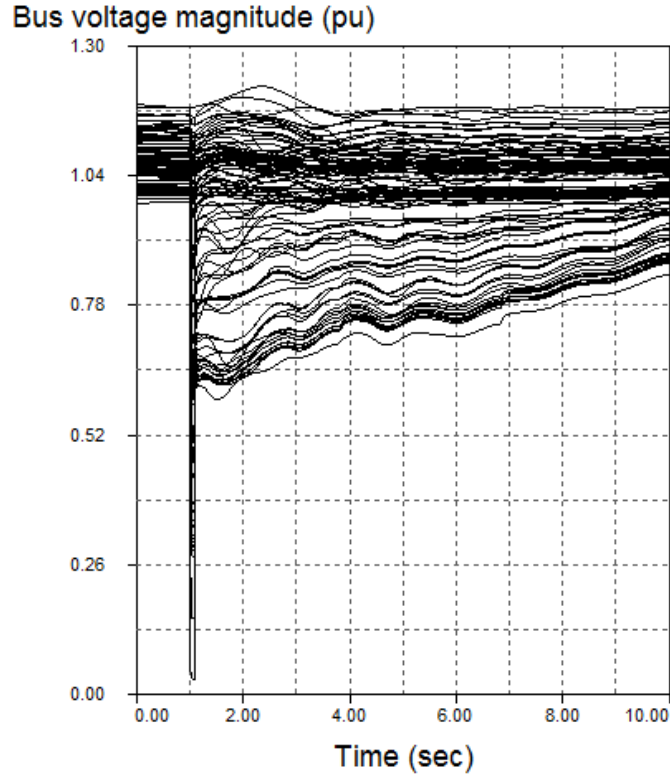
Figure 5.1: Bus Voltages Following 37-64 Fault, HS18

Using the load voltage and load current values from this case, the Z Deviation at each load bus was calculated. The load voltages and load currents were obtained for this fault and used to calculate the Z Deviation at each load bus. There were some significant deviations in load impedance magnitude, including a number of buses with a deviation greater than 50%. Table 5.1 lists the highest Z Deviations at 1.5 seconds.

These results lend credence to the proposal that a significant increase in Z Deviation across the system can be used to identify an FIDVR event. Implementing control methods considerably increases the short term voltage recovery following this fault. Fig. 5.2 shows the system bus voltages for the same fault, but with 30% system wide UVR implemented in the A/C motors. As previously stated, this percentage is optimistic.

44

Table 5.1: 37-64 Fault HS18 Z Deviation Percentage

37-64 Fault HS18 Z Deviation Percentage @ 1.5s	
Bus Number	Z Deviation Percentage
136	62.04805985
151	61.01135744
145	60.39346157
142	60.38606247
152	59.66568258
150	59.49141081
144	58.54633998
61	58.07396474
48	57.89743181
109	57.86294402
137	57.81771171
154	57.76413636
139	57.29030806
51	47.92960782
59	46.51263367
62	46.37345267
54	46.16062907
41	46.01854908
58	45.92889567
57	45.91424448
50	45.85799376
55	45.82721704
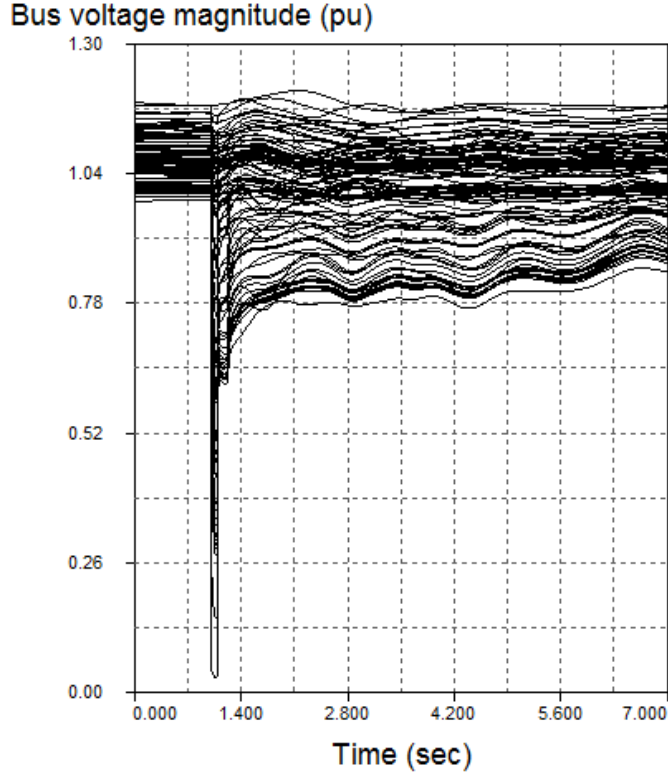
Figure 5.2: Bus Voltages Following 37-64 Fault, 30% UVR

Fig. 5.3 shows the system bus voltages for the same fault with Z Deviation Control implemented. The threshold used for this case was that load is dropped at each bus with a Z Deviation greater than 45%. This threshold was based on results from numerous simulations. As previously mentioned, this involves dropping the same level of load as UVR (30%) at the buses at which it is implemented. As with UVR, the system voltage recovery is greatly improved using this control method.

Note that the simulations are shown only to 7 seconds because that is the nearest second to the point when all buses have met the 80% bus voltage recovery. Both control methods result in a recovery of system bus voltages to greater than 80% pre-fault levels, which is in line with the standards used for this research. A comparison of the voltage recovery can be seen in Table 5.2, which lists the ten highest voltage deviations for each method at 7 seconds.

46
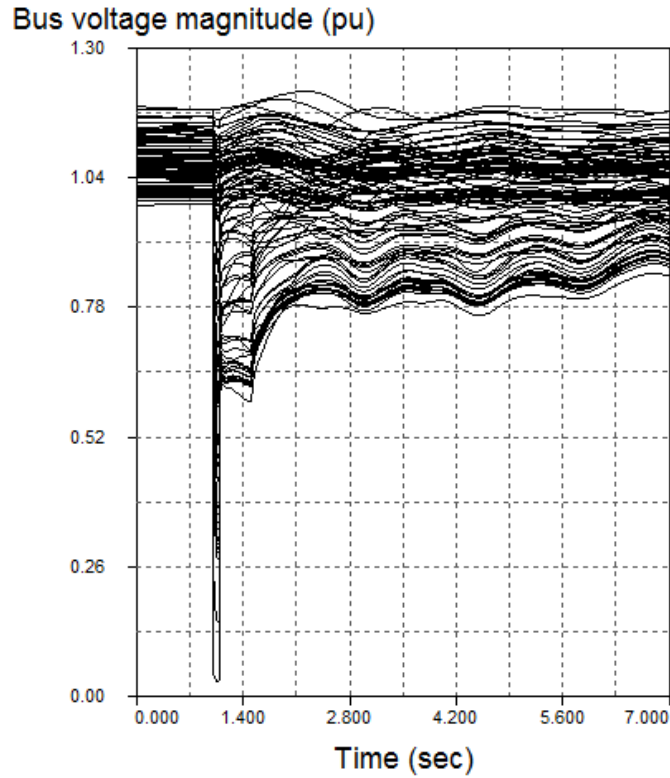
Figure 5.3: Bus Voltages Following 37-64 Fault, Z Deviation Control

Table 5.2: UVR and Z Deviation Control Voltage Recovery, 37-64 Fault

37-64 Fault Control Method Voltage Recovery (7s)			
Bus Number	UVR Volt. Dev. %	Bus Number	ZD Volt. Dev. %
150	16.7317445	51	17.3607676
51	16.43891085	54	17.0348358
54	16.23282412	150	16.8532386
41	16.04615717	41	16.8375216
55	15.99966526	55	16.7683382
59	15.95904862	59	16.7438476
57	15.93871212	62	16.6953652
58	15.93758131	58	16.6845016
61	15.91342869	57	16.6772404
62	15.90826813	50	16.5710766

As can be seen, UVR results in a slightly greater voltage recovery than Z Deviation Control. However, note the difference in total load dropped between the two as given in Table 5.3 comparing the load dropped in each case below.

Table 5.3: Load Drop Comparison, 37-64 Fault

37-64 Fault Load Drop Comparison (7s)		
UVR	Z Deviation	Percent Improvement
1150.64 MW 233.65 MX	991.89 MW 201.41 MX	13.80 %

Z Deviation Control achieves a similar voltage recovery to UVR while shedding 13.80 % less load. It is also important to note that UVR trips at 1.2 seconds, while Z Deviation Control trips later at 1.5 seconds. This difference in implementation time can partially explains the difference in voltage recovery between the methods. As both methods meet the 80% recovery standard, both methods are shown to be viable in improving voltage recovery. In cases that such a small difference in voltage recovery is not vital, Z Deviation Control can accomplish a sufficient recovery while shedding less load.

5.3.2 108-133 Fault

The fault from Bus 108-133 occurs away from the 37-64 fault (north based on the 179 Bus System figure in Chapter 3) but still near the same concentration of high A/C buses. As in the previous case, there are a significant number of buses with delayed recoveries as a result of this fault. This indicates that, at least in this system, that there are certain buses and/or areas that are more susceptible to FIDVR events. The system voltage response following this fault can be seen in Fig. 5.4.
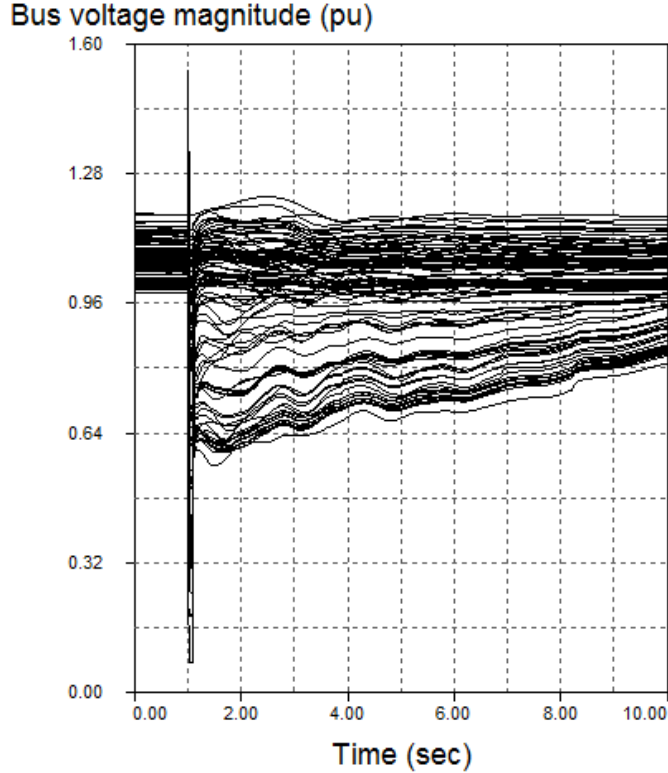
Figure 5.4: Bus Voltages Following 108-133 Fault, HS18

Again, there are a significant number of buses with high Z Deviations, with a several more than 50%. Many of the same buses that had high Z Deviations following the 37-64 fault have a high Z Deviation following this fault. However, the values and order are different. Table 5.4 lists the highest Z Deviations for this case at time 1.5 seconds.

Implementing UVR greatly improves the voltage recovery, with all buses having recovered to the 80% threshold by 6 seconds post fault. The voltage response can be seen in Fig. 5.5.

As in the previous case, Z Deviation control was implemented for all buses with a Z Deviation greater than 45%. Just as in the previous fault, this threshold was selected based on results from numerous simulations. Again, this method showed an improved voltage recovery, with all buses recovering to the standard threshold within 6 seconds post-fault. The voltage response for this method can be seen in Fig. 5.6.

Table 5.4: 108-133 Fault HS18 Z Deviation Percentage

108-133 Fault HS18 Z Deviation Percentage @1.5s	
Bus Number	Z Deviation %
136	62.15420133
142	60.81011248
145	60.68691408
151	59.87554624
152	59.84903163
150	58.98165187
109	58.90136297
154	58.87151823
137	58.84678546
61	58.64097509
144	58.52109783
48	58.35997058
139	57.18498422
143	55.58260299
51	48.77012541
59	47.65732364
62	47.45389775
102	47.10246106
54	46.8736008
41	46.8026406
58	46.68877165
57	46.63245187
55	46.63097453
50	46.57953793

Figure 5.5: Bus Voltages Following 108-133 Fault, 30% UVR
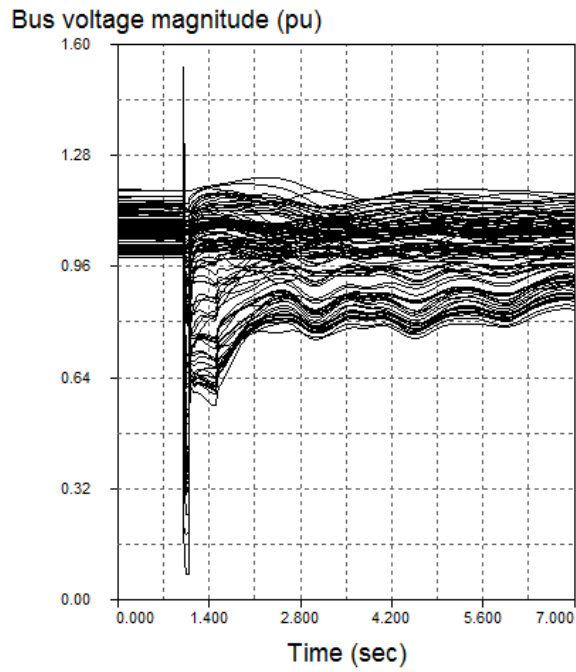
Figure 5.6: Bus Voltages Following 108-133 Fault, Z Deviation Control

51

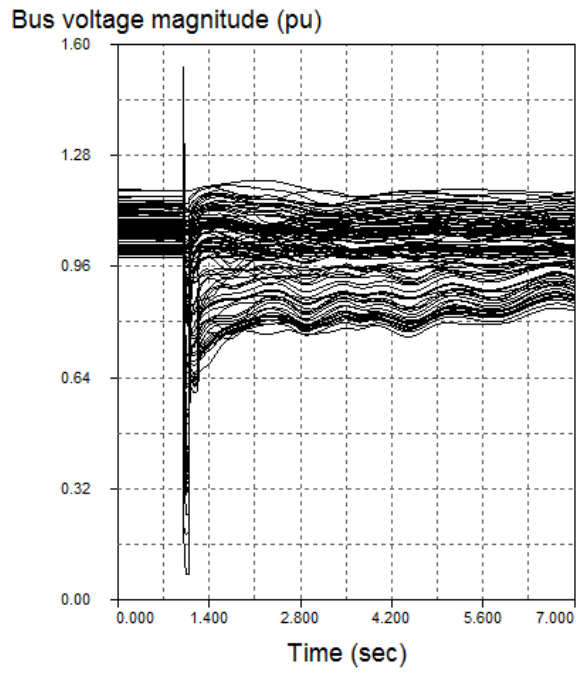**Table 5.5:** UVR and Z Deviation Control Voltage Recovery, 108-133 Fault

108-133 Fault Control Method Voltage Recovery (7s)			
Bus Number	UVR Volt. Dev. %	Bus Number	ZD Volt. Dev. %
150	17.66563862	150	17.47827086
51	17.57804461	51	17.12660631
54	17.3354296	54	16.9156753
41	17.14322288	41	16.71481249
55	17.10979333	55	16.65939586
59	17.03577639	57	16.61034945
58	17.02190988	59	16.60455917
57	17.01294219	58	16.60437645
62	17.00096439	61	16.57708399
61	16.97570295	62	16.55720063

Table 5.6: Load Drop Comparison, 108-133 Fault

108-133 Fault Load Drop Comparison (7s)		
UVR	Z Deviation	Percent Improvement
1150.64 MW 233.65 MX	1019.26 MW 206.97 MX	11.42 %

The simulations for UVR and Z Deviation are shown to 7 seconds as it is the nearest second when all buses have recovered to at least 80% pre-fault voltage. A comparison of the two control methods can be seen in Table 5.5.

In this case, the voltage recovery is greater at 7 seconds utilizing Z Deviation Control than with UVR. However, it is important to note that the recovery of bus voltages in this fault was not a constant increase from the time control was implemented, but there is some swing. The voltage recovery of Bus 150 for both control methods following this fault in Fig. 5.7 is used to illustrate this. Note the difference of the two control schemes, as the recoveries are remarkably similar, but Z Deviation Control recovers slightly slower. Regardless, it can be seen that both methods provide similar and sufficient voltage recovery. A comparison of the load dropped in each method can be seen in Table 5.6.
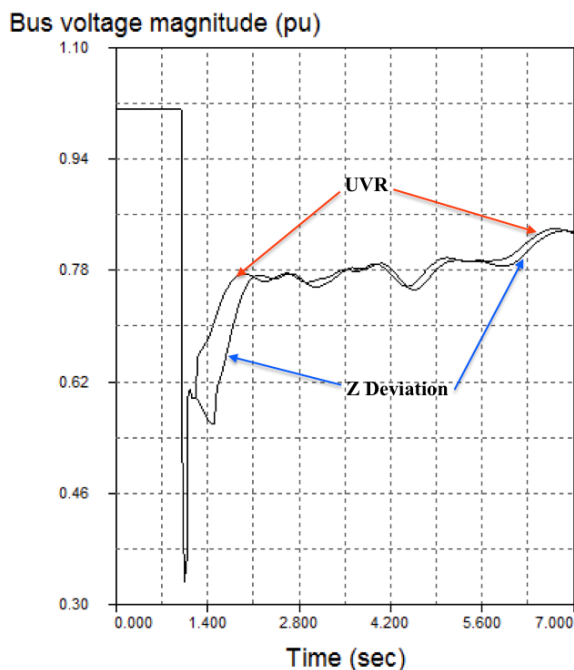
Figure 5.7: Bus 150 Voltage Recovery, 108-133 Fault

The load dropped via UVR in both the 37-64 and 108-133 faults is the same, indicating that it tripped in the same buses in both instances. This shows that although the two faults occur in different areas, the proximity of the two faults to the same concentration of load buses with high A/C causes a similar response. Z Deviation Control, however, drops more load in this instance than previously. Despite this, Z Deviation Control still drops 11.42% less load than UVR for a similar level of voltage recovery.

5.3.3   14-26 Fault

The fault from Bus 14-26 occurs closer to the edge of the system near the generator at Bus 4 (southeast corner in the figure), but still in moderate proximity to the concentration of high A/C buses seen in the previous two faults. The voltage response to this fault can be seen in Fig. 5.8. In the immediate time following the fault, the voltage recovery for most buses is more rapid than in the previous two cases, with the exception of Bus 2, which stays suppressed for most of the simulation. This case

does, however, meet the performance criteria of FIDVR used in this thesis, as Bus 136 has a voltage deviation greater than 20% at 3 seconds, or 2 seconds post-fault. A list of voltage deviations for this fault can be seen in Table 5.7.
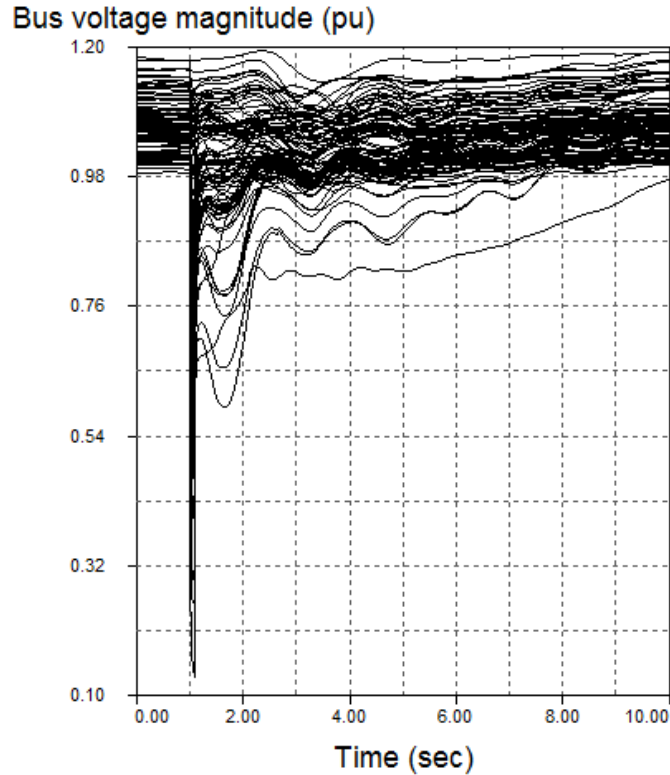
Figure 5.8: Bus Voltages Following 14-26 Fault, HS18

The Z Deviation values following this fault can be seen in Table 5.8. As in the previous cases, there are several buses with Z Deviations greater than 50%. In this case, there is a more stark drop in Z Deviation from buses with significant percentages to more moderate, as seen in the difference in percentage between buses 139 and 142. There are also some buses experiencing high Z Deviation that have not been present in the previous two cases, i.e., buses 2, 8, 10, 12, 16 and 19. These are in a different area than the concentration experiencing FIDVR in the previous two cases, showing FIDVR is a concern in multiple areas in this system.

The voltage response with UVR implemented is given in Fig. 5.9. As in previous cases, it increases the voltage recovery of the system.

54

Table 5.7: 14-26 Fault HS18 Voltage Deviation Percentage

14-26 Fault Voltage Deviation % (3s)	
Bus Number	Voltage Dev. %
136	21.33128253
152	18.88192401
2	17.6353439
16	14.427684
19	14.07395439
151	13.59929183
145	8.916866034
142	8.538600857
15	8.394388797
139	8.079041073

Table 5.8: 14-26 Fault HS18 Z Deviation Percentage

14-26 Fault HS18 Z Deviation Percentage (1.5s)	
Bus Number	Z Deviation %
136	62.92297085
12	62.62415355
8	62.36961709
2	61.74849208
10	61.2695432
19	60.98578855
16	60.63937539
152	59.05092211
151	58.40693462
139	58.27678331
142	23.54520687
145	21.93214055
4	18.96263982
15	16.65558576
51	15.81719289
154	15.31528789
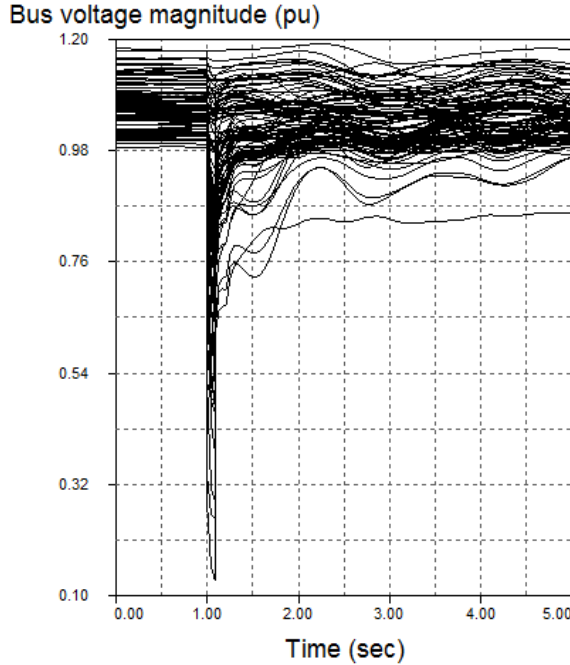
Figure 5.9: Bus Voltages Following 14-26 Fault, 30% UVR

The system voltage response of the system with Z Deviation Control is given in Fig. 5.10. The Z Deviation sees a stark drop-off; the threshold for Z Deviation Control could have been set at a number of values. For consistency with the other simulations, the threshold for this case was again set to 45%.

In both cases, the recovery of the voltages to 80% occurs sooner than in the previous. Thus, the simulations are shown and deviation levels are compared at 5 seconds here. While slightly more difficult to see in the graph, as some of the buses still recover slowly, there is a marked improvement in voltage recovery through use of these techniques. The voltage recovery comparison in Table 5.9 shows this improvement more clearly.

As in the previous cases, both methods result in sufficient voltage recovery, and the levels of recovery are similar. Table 5.10 shows the load drop comparison.

The difference in load dropped is even more significant in this case, with Z Deviation Control dropping 31.81% less load. As both cases recover to the 80% threshold, unless a minor recovery in voltage is absolutely necessary, Z Deviation
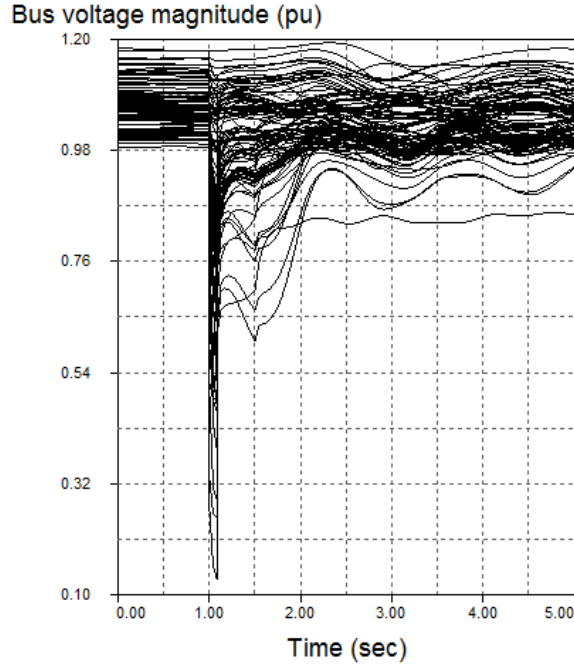
Figure 5.10: Bus Voltages Following 14-26 Fault, Z Deviation Control

Table 5.9: UVR and Z Deviation Control Voltage Recovery, 14-26 Fault

14-26 Fault Control Method Voltage Recovery (5s)			
Bus Number	UVR Volt. Dev. %	Bus Number	ZD Volt. Dev. %
2	13.67984575	2	14.05559303
136	10.86207494	136	12.91399324
152	9.054888043	152	10.97534335
19	7.009311308	19	8.319259119
16	6.478709511	16	7.925808773
151	5.534808295	151	7.132554648
10	5.190383192	10	5.564792114
8	4.862765936	8	5.231377655
164	4.014037118	12	4.195251677
17	3.858737995	17	4.157628361
12	3.412583525	164	4.025777888

Table 5.10: Load Drop Comparison, 14-26 Fault

14-26 Fault Load Drop Comparison (5s)		
UVR	Z Deviation	Percent Improvement
759.05 MW 154.13 MX	517.58 MW 105.10 MX	31.81

Control can accomplish sufficient recovery for a significantly less amount of dropped load. All three analyzed cases have shown that Z Deviation Control is adequate. The simulations have also shown that Z Deviation can be an indicator of an FIDVR event, as all three events had buses with significant deviations. In all three cases, Z Deviation Control shed a lesser amount of load than UVR while giving a similar voltage recovery profile, despite it triggering later.

5.4   Seasonal Analysis

The data from the previous section all resulted from simulations with load compositions based on HS18 data from WECC. This is a time and season with a significant level of A/C load, so the system was vulnerable to FIDVR events, as evidenced in the results. However, it is important to model power systems for a variety of times and seasons, when load composition can differ drastically. Thus, the following section presents an analysis for a different time and season, HW08. This seasonal analysis serves multiple purposes: to observe system response when levels of single phase A/C are lower system wide, and to provide a case for Z Deviation based control that may require significantly different response. The control case will observe if Z Deviation levels differ when A/C penetration is lower and is accurate for identifying FIDVR events, as well as observe if Z Deviation Control can function under highly different conditions.

5.4.1 Fault Analysis

The same faults performed in the previous section, 37-64, 108-133, and 14-26, are performed for a system model with HW08 based load composition. Load composition percentages for this case are given in Appendix B.2. Voltage response to these faults is presented in Fig. 5.11.

Each fault was simulated for the same time as in the HS18 case. As can be seen, the voltage deviation in each case is significantly less with a decreased penetration of A/C, with all bus voltages recovering well past the 80% threshold outlined in this paper. In addition, none of the faults meet the requirement for an FIDVR event as outlined earlier in this thesis. Thus, the overall penetration of A/C in a system correlates strongly with the occurrence and severity of FIDVR events. While the voltage deviations are low, it is important to observe the Z Deviations for each fault. Table 5.11 lists the top 5 Z Deviations for each fault with the HW08 model.

There is still deviation in the load impedance of buses in all three faults, with Z Deviations exceeding 30% following the 37-64 and 108-133 faults. These two faults again share similarities with buses showing the highest Z Deviations, suggesting that the same concentration of high A/C penetration buses as with HS18 parameters is still more susceptible to Z Deviation. However, in all three cases, Z Deviation control would not be triggered based on the 45% threshold used for the same faults with the HS18 model. As such, a Z Deviation Control scheme such as that used in the previous section would not lead to unnecessary dropping of load, when voltage recovery is significantly quicker. In addition, the maximum Z Deviations in each case are significantly lower with HW08 parameters than with HS18, and significant Z Deviations are not as prevalent. This leads credence to the notion that seeing a high concentration of significant Z Deviation in a system can be used to identify an FIDVR event.
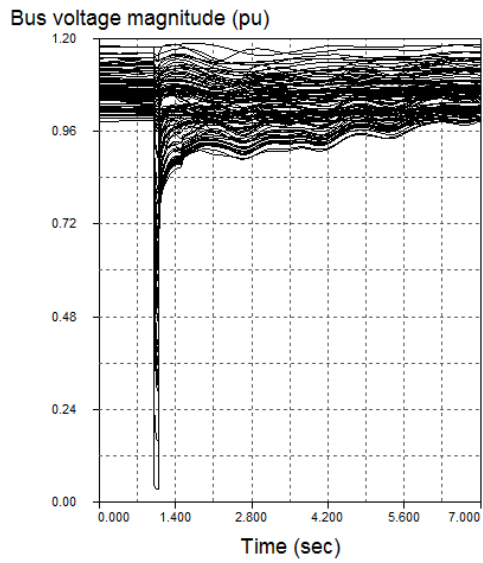
(a) 37-64 Fault
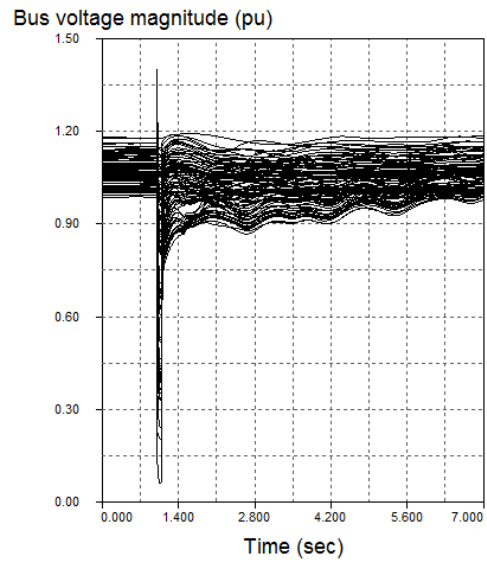
(b) 108-133 Fault
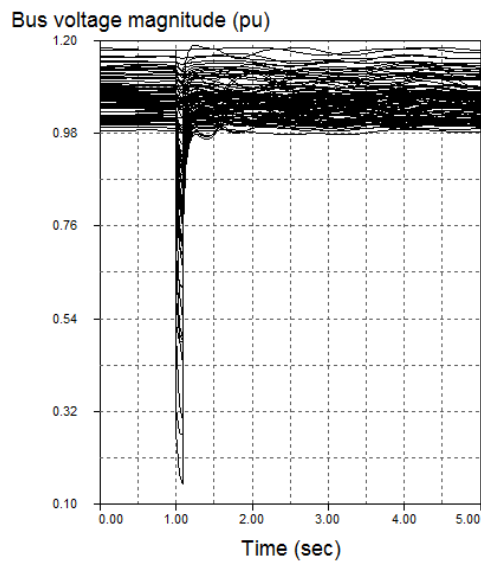
(c) 14-26 Fault

Figure 5.11: Bus Voltage Response, HW08

60

Table 5.11: HW08 Z Deviation Percentage Comparison

37-64 Fault HW08 Z Deviation Percentage (1.5s)	
Bus Number	Z Deviation Percentage
110	33.73607404
150	33.64748677
51	33.55648321
61	33.13937684
48	33.13184999
108-133 Fault HW08 Z Deviation Percentage (1.5s)	
Bus Number	Z Deviation Percentage
110	34.2325611
150	33.66526157
51	33.52829884
107	33.34625476
61	33.1621671
14-26 Fault HW08 Z Deviation Percentage (1.5s)	
Bus Number	Z Deviation Percentage
152	29.49273547
139	27.87857757
136	20.33115636
16	18.13641755
19	17.86542458

5.5 Remarks on Implementation of Load Models

This section clarifies some specific details on the simulations.

5.5.1 Load Drop Comparison

Note that the load drop comparisons used in section 5.3 are short term load drop comparisons. After sufficient time, the percentage of motors unable to restart (the percent not assigned to the frst parameter) will be tripped by the thermal relays modeled by the motors. This dynamic is based upon what WECC research has shown to be a realistic amount of A/C able to restart [25]. Thus at a certain point in simulations, most of the A/C load will be shed in both control scheme cases.

The purpose of the load drop comparison is to show the effectiveness of Z Deviation Control in identifying the most effective load to shed. In all three cases, Z Deviation Control is able to achieve an incredibly similar recovery profile to UVR despite shedding less load and being implemented at a later time. Thus it can be seen that Z Deviation is valuable for identifying problem load, which reinforces that it is a good indicator for FIDVR at a bus.

5.5.2 Z Deviation Control Threshold

As seen in this chapter, the threshold used for dropping load via Z Deviation Control in all three fault cases is 45%. As previously mentioned, this threshold was established based on the results from extensive simulations of the fault cases. However, it is important to try to understand why this threshold performs as well as a control method, and what exactly the 45% threshold signifies. While TSAT has the capability of measuring the speed of the three phase induction motor speeds, it does not have the capability of doing this for just the single phase A/C. Still, from the results of the HW08 case analysis, it can be seen that the highest Z Deviation percentages for all three faults were approximately 34%, 34%, and 29% respectively. In all HW08

cases, these Z Deviations do not correspond to an FIDVR event. Thus, based on this testing, the 45% threshold is at a level high enough that it does not activate at the level of Z Deviation seen in events that do not cause FIDVR. The level may vary between systems.

Chapter 6

Conclusions and Future Work

This thesis studies the occurrence of FIDVR and mitigation methods on a large test system. The 179 bus representation of the WECC system includes a diverse load model consisting of realistic load composition data and motor parameters. Through mathematical analysis and simulation results, a new method, Z Deviation, is proposed as a way to indicate the occurrence of FIDVR at a bus. Further, this method is implemented into a control scheme, Z Deviation Control, used to mitigate the effects of FIDVR and improve the system-wide voltage recovery. Z Deviation Control is compared to simple undervoltage load shedding method used to improve voltage recovery. Both methods improve the voltage recovery profile but Z Deviation Control achieves this with lower load shedding. Based on the work performed in this thesis, it is concluded that significantly high Z Deviation at a number of buses within a system with high residential A/C penetration is a reliable indicator of an FIDVR event. As well, it is concluded that Z Deviation is able to identify the effective load to shed.

Future work based on the research presented in this thesis has numerous possibilities. An optimization study for the load dropped, such as amount and what buses to drop it from, for a Z Deviation based control scheme could be investigated. This could look at an ideal amount of load to drop at certain buses and what the threshold for dropping load should be. Similar tests as those performed in this paper

for a different power system should also be investigated. This could address the value of Z Deviation in areas that have different load profiles, and thus different penetrations of A/C. As efforts increase to implement more renewable generation in the grid, a study of the effect increased renewable penetration has on FIDVR and system wide voltage recovery could also prove valuable.

Bibliography

[1] Prabha Kundur. *Power System Stability and Control.* McGraw-Hill, Inc., 1994. 4, 5, 7, 8, 9, 31, 32, 33, 36

[2] IEEE/CIGRE Joint Task Force on Stability Terms and Definitions. Definition and classification of power system stability. *IEEE Transactions on Power Systems*, 19(2), 2004. 5, 6

[3] Y. Li, H.D. Chiang, B.K. Choi, Y. T. Chen, D. H. Huang, and M. G. Lauby. Representative static load models for transient stability analysis: development and examination. *IET Gener,Transm. Distrib.*, 1(3):422–431, 2007. 8

[4] Dimitri Kosterev, Anatoliy Meklin, John Undrill, Bernard Lesieutre, William Price, David Chassin, Richard Bravo, and Steve Yang. Load modeling in power system studies: Wecc progress update. 9, 10, 11, 12, 13

[5] IEEE Task Force on Load Representation for Dynamic Performance. Load representation for dynamic performance analysis. *IEEE Transactions on Power Systems*, 8(2):472–482, May 1993. 9

[6] IEEE Task Force on Load Representation for Dynamic Performance. Standard load models for power flow and dynamic performance simulation. *IEEE Transactions on Power Systems*, 10(3):1302–1313, August 1995. 9

[7] Bradley R. Williams, Wayne R. Schmus, and Douglas C. Dawson. Transmission voltage recovery delayed by stalled air conditioner compressors. *IEEE Transactions on Power Systems*, 7, 1992. 10, 11, 12, 38

[8] Transmission Issues Subcommittee. A technical refernece paper fault-induced delayed voltage recovery. Technical report, NERC, June 2009. 10, 11, 16, 17

[9] John Kueck, Dmitry Kosterev, John Undrill, and Joseph Eto. Voltage sag and recovery influence for modeling motor loads. *IEEE*, 2014. 10

[10] John W. Shaffer. Air conditioner response to transmission faults. *IEEE Transactions on Power Systems*, 12(2), 1996. 11, 22

[11] Lee Y. Taylor, Robert A. Jones, and S. Mark Halpin. Development of load models for fault induced delayed voltage recovery dynamic studies. *IEEE*, 2008. 12

[12] Les Pereira, Dmitry Kosterev, Peter Mackin, Donald Davies, John Undrill, and Wenchun Zhu. An interim dynamic induction motor model for stability studies in the wscc. *IEEE Transactions on Power Systems*, 17(4), 2002. 12

[13] Bernard Lesieutre, Dmitry Kosterev, and John Undrill. Phasor modeling approach for single phase a/c motors. *IEEE*, 2008. 13

[14] Load Model Task Force. Wecc dynamic composite load model specifications. Technical report, WECC, January 2015. 13

[15] Ryan D. Quint. A look into load modeling: The composite load model. *Dynamic Load Modeling and FIDVR Workshop*, 2015. 13

[16] Peak Reliability. *CIP-014-1 Guideline*. 14, 42

[17] Transmission Planning Department. Exelon transmission planning criteria. 2009. 15

[18] Hua Bai. *Novel measurement based load modeling and demand side control methods for fault induced delayed voltage recovery mitigation*. PhD thesis, Iowa State University, Ames, Iowa, 2010. 16, 37, 38

[19] Yun-Hwan Lee, Bo-Hyun Park, Seung-Chan Oh, Byong-Jun Lee, Jeong-Hoon Shin, and Tae-Kyun Kim. Implementation of under voltage load shedding for fault induced delayed voltage recovery phenomenon alleviation. *Journal of Electrical Engineering and Technology*, 9(2):406–414, 2014. 16

[20] Daniel Sullivan, Ron Pape, Joe Birsa, and Mike Riggle et al. Managing fault-induced delayed voltage recovery in metro atlanta with the barrow county svc. *IEEE*, 2009. 17

[21] Daniel Sullivan, John Paserba, Gregory Reed, Terry Croasdaile, Ron Pape, and Donald Shoup et al. Design and application of a static var compensator for voltage support in the dublin, georgia area. *IEEE*, 2006. 17

[22] N. Lu, B. Yang, Z. Huang, and R. Bravo. The system impact of air conditioner under-voltage protection schemes. *IEEE*, 2009. 18, 41

[23] Powertech Labs Inc. *TSAT Model Manual*. Surrey, British Colombia, April 2014. 20

[24] Load Model Task Force. Wecc load composition data. 21, 23

[25] Richard Bravo, Jun Wen, Dmitry Kosterev, Bill Price, and Robert Yinger. Wecc air conditioner motor model test report. Technical report, WECC, 2014. 21, 62

[26] Slava Maslennikov, Bin Wang, Qiang Zhang, Feng Ma, Xiaochuan Luo, Kai Sun, and Eugene Litvinov. A test cases library for methods locating the sources of sustained oscillations. 23

[27] Dimitry Kosterev. Composite load model development and implementation. *NERC-DOE FIDVR Conference*, 2015. 23

Appendix

Appendix A

Motor Dynamic Models

A.1 Single Phase A/C Model Parameters

Single Phase A/C Parameters		
Parameter	**Value**	**Description**
CompLF	1	Compressor Load Factor
Tv	0.025	Voltage Input Time Constant
Tf	0.05	Frequency Input Time Constant
CompPF	0.98	Compressor Power Factor
Vstall	0.6	Compressor Stall Threshold Voltage
Rstall	0.124	Compressor Stall Resistance
Xstall	0.114	Compressor Stall Reactance
Tstall	0.033	Stall Time
LFadj	0.3	Vstall Adjustment Proportional to Loading Factor
Kp1	0	Real Power Coefficient, Running State 1
Np1	1	Real Power Exponent, Running State 1
Kq1	6	Reactive Power Coefficient, Running State 1
Nq1	2	Reactive Power Exponent, Running State 1
Kp2	12	Reactive Power Coefficient, Running State 2

Single Phase A/C Parameters cont.		
Parameter	**Value**	**Description**
Np2	3.2	Real Power Exponent, Running State 2
Kq2	11	Reactive Power Coefficient, Running State 2
Nq2	2.5	Reactive Power Exponent, Running State 2
Vbrk	0.86	Compressor Motor Breakdown Voltage
Frst	0.2	Fraction of Motors to Restart
Vrst	0.6	Motor Restart Voltage
Trst	0.4	Motor Restart Time
CmpKpf	1	Real Power Frequency Sensitivity
CmpKqf	-3.3	Reactive Power Frequency Sensitivity
Vc1off	0.45	Voltage 1 @ which Contactors Disconnect the Load Gradually
Vc2off	0.35	Voltage 2 @ which Contactors Disconnect the Load Gradually
Vc1on	0.5	Voltage 1 @ which Contactors Reconnect the Load Gradually
Vc2on	0.4	Voltage 2 @ which Contactors Reconnect the Load Gradually
Tth	10	Compressor Motor Heating Time Constant

Single Phase A/C Parameters cont.		
Parameter	**Value**	**Description**
Th1t	0.7	Temperature @ which Motors Start Tripping
Th2t	1.9	Temperature @ which All Motors are Tripped
fuvr	0	Fraction of Motors w/ Undervoltage Relays
uvtr1	0.8	First Undervoltage Pickup Level
ttr1	0.2	First Undervoltage Pickup Time
uvtr2	0.9	Second Undervoltage Pickup Level
ttr2	5	Second Undervoltage Pickup Time

A.2 Motor A Model

Motor A Parameters		
Parameter	Value	Description
MVA	-0.75	Machine Base MVA (Load Factor when Negative)
T'	0.095	Transient Open Circuit Time Constant
T"	0.0021	Subtransient Open Circuit Time Constant
H	0.1	Inertia Constant
X	1.8	Synchronous Reactance
X'	0.12	Transient Reactance
X"	0.104	Subtransient Reactance
Rs	0.04	Stator Resistance
X1	0.132	Saturation Reactance
E1	0	Voltage for the Point of the Saturation Characteristic
S(E1)	0	Saturation Coefficient
E2	0	Voltage for the Point of the Saturation Characteristic
S(E2)	0	Saturation Coefficient
LOAD	1	Load Characteristic Flag
A	1	Coefficient in Saturation Characteristic
B	0	Coefficient in Saturation Characteristic
K	0	Damping Coefficient

A.3 Motor B Model

Motor A Parameters		
Parameter	Value	Description
MVA	-0.75	Machine Base MVA (Load Factor when Negative)
T'	0.2	Transient Open Circuit Time Constant
T"	0.0026	Subtransient Open Circuit Time Constant
H	0.5	Inertia Constant
X	1.8	Synchronous Reactance
X'	0.19	Transient Reactance
X"	0.14	Subtransient Reactance
Rs	0.03	Stator Resistance
X1	0.083	Saturation Reactance
E1	0	Voltage for the Point of the Saturation Characteristic
S(E1)	0	Saturation Coefficient
E2	0	Voltage for the Point of the Saturation Characteristic
S(E2)	0	Saturation Coefficient
LOAD	1	Load Characteristic Flag
A	1	Coefficient in Saturation Characteristic
B	0	Coefficient in Saturation Characteristic
K	0	Damping Coefficient

Appendix B

Load Composition Data

B.1   HS18 Load Composition Data

HS 18 Load Composition Data				
Load	Motor A %	Motor B %	Residential A/C %	Electronic Load %
NWC Mix	12.9	12.2	8.6	17
NWC Res.	5.8	8.5	14.5	17.3
NWV Mix	14.5	14.8	17.3	15.9
NWI Mix	17.5	14.6	20.8	13.2
NWI Rag.	14.2	13.3	20.3	11.9
RMN Mix	11.8	11.9	9.9	21.1
NCC Mix	14.9	13.5	14.2	17.4
NCV Mix	20.2	15.3	24	12.9
HID Mix	13.6	15.4	23.2	13.4
HID Res.	6.1	14.4	39.1	12.5
SCC Mix	11	12.8	14.7	17.6
SCV Mix	14	15.8	25.2	13
SCI MIx	12.5	15.5	23.6	13.8
DSW Mix	15.7	16.2	26.6	11.6
PPA_AUX	5	50	0	15

B.2   HW08 Load Composition Data

HS 18 Load Composition Data				
Load	Motor A %	Motor B %	Residential A/C %	Electronic Load %
NWC Mix	6.6	11.3	9.9	9.1
NWC Res.	2.4	9.4	13.9	5.9
NWV Mix	7	12.7	9.5	10.2
NWI Mix	10	11.1	9.6	9.1
NWI Rag.	11.5	10.5	10	7.5
RMN Mix	9.6	13.9	8	10.7
NCC Mix	6.7	14.3	8.8	12
NCV Mix	7.6	13.2	8.4	13
HID Mix	7.4	15.7	7.5	12.2
HID Res.	2.9	15.4	12	9.1
SCC Mix	7.2	13.8	6.5	14.3
SCV Mix	7.7	14.1	7	13.7
SCI MIx	7.2	14.3	7.1	13.6
DSW Mix	8.7	10.3	3.6	16.3
PPA_AUX	5	50	0	15

Vita

Derek Lusby was born in Knoxville, TN, to parents David and Beth Lusby. He attended South-Doyle High School where he was named Valedictorian. Following graduation, he enrolled at the University of Tennessee, Knoxville, where he majored in Electrical Engineering. He graduated Magna Cum Laude in Spring 2015 with his Bachelor's Degree. He then enrolled in graduate school to pursue his Master's Degree at the University of Tennessee, where he majored in Power Systems. While in graduate school, he was a Graduate Teaching Assistant for the EECS Senior Design classes for Fall 2015 and a Graduate Research Assistant starting in Spring 2016. His research focused on Fault Induced Delayed Voltage Recovery